Kumiko Mackasey

Evaluating Angiotensin II Type 1 Receptor Changes in Post- Renal Insufficiency and in Left Anterior Descending Artery Ligation Animal Models Using [^{11}C]Methyl-Candesartan

This thesis is submitted as a partial fulfillment of the
Master of Science program in Cellular and Molecular Medicine
2012

Supervisors: Dr. Jean DaSilva, PhD and Dr. Rob Beanlands, MD, FRCPC

Table of Contents

Acknowledgements

I would like thank the following people for their contributions to my project:

- Stephanie Thorn: Animal Surgeries, Echocardiography
- PET Radiochemistry Group (Jeff Collins, Julian Walcott, Keegan Flowers, Tayabeh Hadizad): PET tracer synthesis
- Myra Kordos: PET imaging technician
- PET Physics Group (Dr. Rob DeKemp, Chad Hunter Dr. Ran Klein, Jennifer Renaud, Mireille Lortie): PET image analysis software
- PET Biology (Marika Kolajova, Basma Ismail): Confirmation of in vitro results

I would also like to extend my gratitude to my supervisors, Drs. Jean DaSilva and Rob Beanlands for their guidance and insight as well as my lab mates, Dr. Miran Kenk, James Thackeray, Basma Ismail, and Natasha Arksey for their friendship and support.

Abstract

Non invasive *in vivo* imaging will lead to better understanding of Angiotensin II Type 1 Receptor's (AT_1R) role in disease progression and may guide therapy in cardiovascular patients. Two models were used in this project: 5/6 nephrectomy and transient left anterior descending (LAD) ligation. Rats were scanned with [^{13}N]ammonia and [^{11}C]methyl-candesartan, both of which are Positron Emission Tomography (PET) tracers, at 8 weeks (nephrectomy) and 2 weeks (LAD ligation) after surgery. Western blot analysis was used to corroborate PET data. Nephrectomy: Renal AT_1R image analysis displayed a 40% decrease in kidney AT_1R in nephrectomized animals compared to sham ($p<0.05$) which was confirmed with Western blot and biodistribution. LAD ligation: Left Ventricle AT_1R Western blot analysis exhibited a 60% increase in 20min ligation ($p<0.05$) with maintained myocardial blood flow. In conclusion, changes in renal AT_1R were successfully imaged using [^{11}C]methyl-candesartan in nephrectomized animals, and 20min LAD ligation/reperfusion is an appropriate model to image an increase in cardiac AT_1R following ischemic injury.

List of Abbreviations

ACE: Angiotensin Converting Enzyme
ACEi: Angiotensin Converting Enzyme Inhibitor
ANGI: Angiotensin I
ANGII: Angiotensin II
ARB: Angiotensin II Type 1 Receptor Blocker
AT_1R: Angiotensin II Type 1 Recptor
Bq: Bequerel
BW: Body Weight
CKD: Chronic Kidney Disease
ddH_20: Deionized Water
DV: Distribution Volume
EF: Ejection Fraction
EGFR: Epidemial Growth Factor Receptor
EIA: Enzyme Immunoassay
FS: Fractional Shortening
GAPDH: Glyceraldehyde 3-phosphate dehydrogenase
GPCR: G Protein Coupled Receptor
GRK: GPCR Kinase
GTPase: GPCR Phosphotase
HW: Heart Weight
IRW: Inveon Research Workplace
KW: Kidney Weight
LA: Left Atrium
LAD: Left Anterior Descending Coronary Artery
LK: Left Kidney
LV: Left Ventricle
MBF: Myocardial Blood Flow
Me-CN: Methyl-candesartan
MI: Myocardial Infarct (Permanent Occlusion)
Nx: Nephrectomy
PET: Positron Emission Tomography
PPARγ: Peroxisome Proliferator Activated Receptor γ
PVE: Partial Volume Effect
RAS: Renin-Angiotensin System
RBF: Renal Blood Flow
ROI: Region of Interest
SPECT: Single Photon Emission Computer Tomography
TGF: Transforming Growth Factor
TM: Transmembrane
TRV: Test Retest Variability

List of Tables

List of Figures

1. Introduction

1.1 Renin Angiotensin System

The Renin Angiotensin System (RAS) is a regulator of sodium balance, vascular resistance and extracellular volume. This pathway is activated in response to decreased blood pressure, decreased sodium intake, and increased stress and trauma (Harrison-Bernard 2009). Angiotensinogen is a peptide produced in the liver and cleaved by renin, produced primarily in the kidney, to produce Angiotensin I (ANGI) which is then converted to Angiotensin II (ANGII) by Angiotensin Converting Enzyme (ACE) or to a lesser extent, by chymase. ACE is a membrane bound protein that is found in the endothelial cells, neuroepithelial cells and renal proximal convoluted tubule cells. The RAS is an endocrine system; however, tissues such as the heart, brain and kidney produce components of the system which suggests a role of locally produced ANGII in the function of these tissues (Dostal et al. 1999).

ANGII binds to at least 3 different receptors, AT_1R, AT_2R and AT_4R (Berk 2003). The most understood and physiologically important of these receptors is the AT_1R which will be the focus of this thesis. AT_1Rs are expressed in heart, brain, kidney, gut, adrenal and vascular tissue, with a high abundance in kidney and adrenal glands (Timmermans et al. 1992; Goodfriend et al. 1996; Allen et al. 1999; Dostal et al. 1999; Allen et al. 2000; De Gasparo et al. 2000; Opie et al. 2001; Gard 2002; Wagenaar et al. 2002; Li et al. 2003). ANGII, when bound to AT_1R, will initiate mechanisms that will increase contractile force of the heart, hypertrophy, fibrosis, vascular tone, constriction of vessels, reabsorption of sodium in the kidney, and production of reactive oxygen species (Bayorh et al. 2005;

Ferrario 2009) (Fig 1). While AT_1R is dominant in adult tissues, AT_2R is the main ANGII receptor in fetus. AT_2R may be expressed in response to disease (Masaki et al. 1998; Akishita et al. 2000). AT_2R is documented as having the opposite downstream effects to AT_1R; it promotes apoptosis, inhibits growth, lowers blood pressure and reduces inflammation (Nakajima et al. 1995; Masaki et al. 1998). Although less is known of the AT_4R, it is present in endothelial cells and its possible role is to control expression of procoagulant species (Senchenkova et al. 2010)

1.1.1. AT_1R

The AT_1R is a G-protein coupled receptor (GPCR) which upon agonist binding is desensitized and internalized similarly to other GPCRs. The AT_1R acts through second messengers to promote downstream effects such as vasoconstriction, inflammation, atherogenicity, cellular proliferation and matrix production.

The receptor has seven transmembrane domains and is composed of 359 amino acids (Fig 2) with a molecular weight of 41 kDa (De Gasparo et al. 2000). The extracellular region is composed of an N-terminus and three extracellular loops. These loops consist of three N-glycosylation sites and four cysteine residues. Each glycosylatation site is glycosylated in the native AT_1R. The glycosylated AT_1R has a molecular weight of 65 kDa (De Gasparo et al. 2000). All GPCRs have 2 cysteine residues which form a disulfide bond between the first and second extracellular loop. AT_1R has an additional pair of cysteines to form another disulfide bond which maintains the shape of the receptor (Ohyama et al. 1995). The second disulfide bond makes AT_1R susceptible to inactivation by reducing agents and is not present in the AT_2R. The

cytoplasmic region

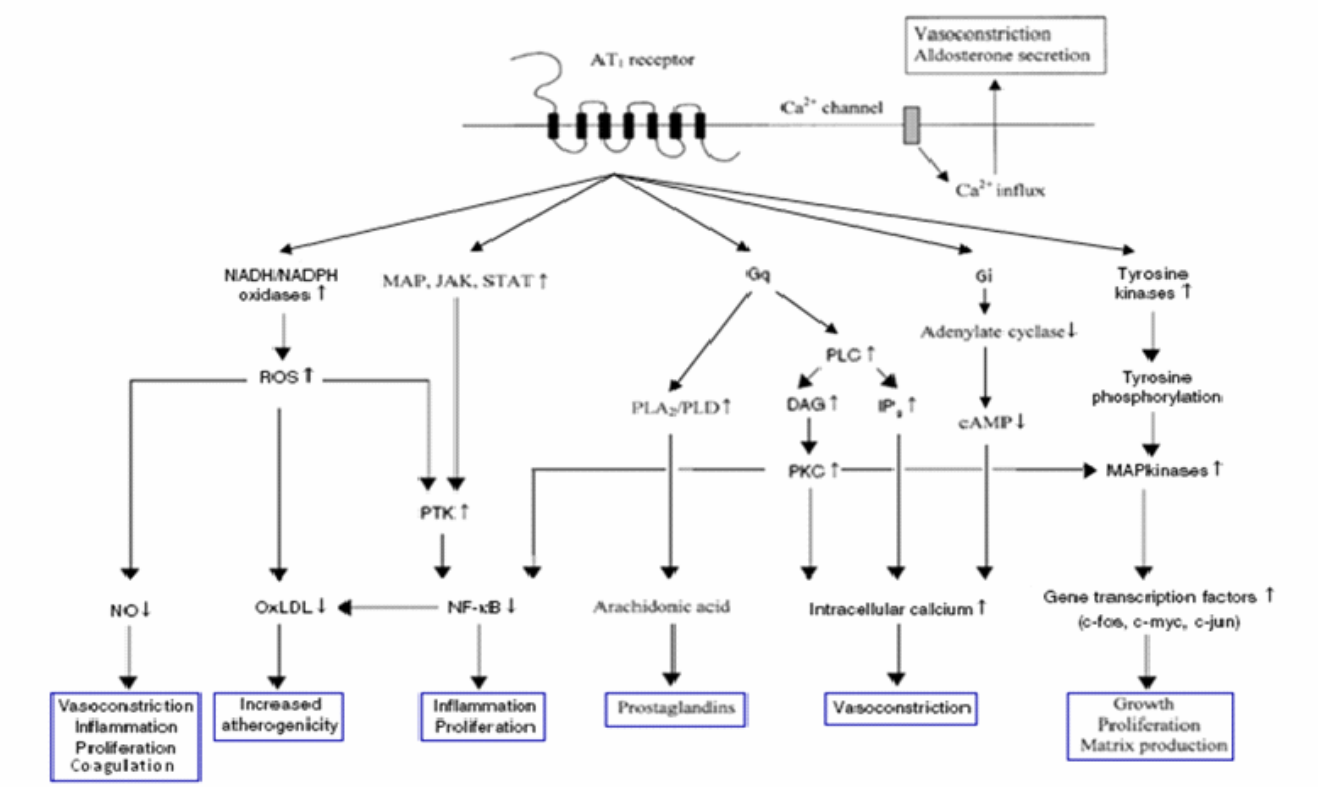

Figure 1: Intracellular downstream effects of ANGII binding to AT_1R. Upon ANGII binding, AT_1Rdownstream effects include: vasoconstriction, inflammation and growth. (Adapted from(Dinh et al. 2001); (Wagenaar et al. 2002).

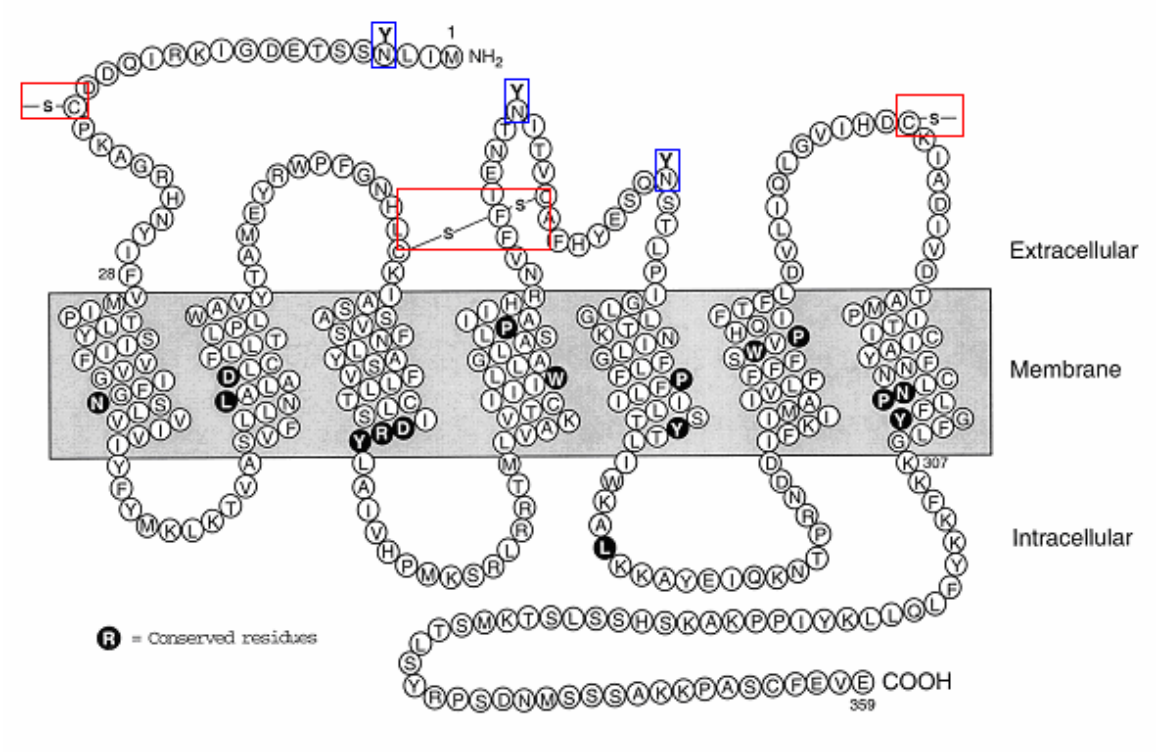

Figure 2: Amino acid structure and configuration of mammalian AT_1R (De Gasparo et al. 2000). AT_1R is a seven transmembrane GPCR protein composed of 359 amino acids. Red rectangles outline the location of disulfide bonds; blue rectangles highlight substrates for N-glycosylation.

contains three intracellular loops and a C-terminus cytoplasmic tail. Phosphorylation sites are present on the intracellular region.

While most mammalian species have only one form of the AT_1R, mice and rats have two forms of the receptor, $AT_{1A}R$ and $AT_{1B}R$. The amino acid sequences of these two forms of the receptor are 95% identical (Kakar et al. 1992). The subtypes are similar in terms of ligand binding and activation properties, but differ in tissue distribution, chromosomal location and transcriptional regulation. A suggested explanation of the presence of two subtypes in rats and mice is that AT_1R duplicated during evolution after the branching of rodents (Aiyar et al. 1994).

$AT_{1A}R$ mRNA is most prominent in all tissues with the exception of adrenal and pituitary glands, where $AT_{1B}R$ is dominant. $AT_{1A}R$ is expressed in the kidney, heart, liver, adrenal gland, brain, lung, fat and gonads. $AT_{1B}R$ expression is limited to adrenal gland, pituitary gland, brain and testis in the adult mouse (Burson et al. 1994). In the kidney of adult male rat, 73% of AT_1R are $AT_{1A}R$ (Llorens-Cortes et al. 1994). From here on, subtypes of AT_1R will not be differentiated. Human and rat AT_1R share 95% homology (De Gasparo et al. 2000).

1.1.2 AT_1R Signaling

ANGII has high affinity for AT_1R by maintaining multiple points of contact with the receptor. Interactions between the Tyr^4 residue in ANGII and Asn^{111} in transmembrane (TM) domain 3 of AT_1R and Phe^8 of ANGII and His^{256} of TM6 of the receptor are required to fully convert the receptor to its activated form (Noda et al. 1995; Noda et al. 1996). Upon binding of the agonist to the receptor, a conformational change is induced and transmitted to the intracellular C-terminus which then interacts with the G protein. $G_{q,}$ the main G protein associated with AT_1R, activates phospholipase-C β1 (PLC β1) which in turn activates protein kinase-C causing a release of Ca^{2+} from intracellular stores, increasing cell contractility (De Gasparo et al. 2000) (Fig 1).

In addition to AT_1R's interaction with G proteins, it also activates intracellular pathways, such as MAPK and JAK/STAT mechanisms (Fig 1). ANGII binding to AT_1R causes phosphorylation of PLCγ which cleaves PIP2 to produces IP3 and DAG. IP3 leads to increased intracellular Ca^{2+} and DAG activates PKC which goes on to phosphorylate downstream cascades that promote vasoconstriction and growth (Bernstein et al. 1996). ANGII mediated activation of downstream cascades such as JAK2/STAT are dependent on PLC action (Mehta et al. 2007). GPCRs have no intrinsic phosphorylation ability, therefore another kinase must be involved in the phosphorylation of PLCγ, however this kinase has not been identified. MAPK and JAK/STAT pathways lead to phosphorylation in the nucleus of other kinases and transcription factors that promote cell proliferation and differentiation.

AT_1R has also been shown to transactivate other receptors. Activation of epidermal growth factor receptor (EGFR) involves a Ca^{2+} dependent phosphorylation of the receptor; intracellular Ca^{2+} which is increased by AT_1R activation (Fukai et al. 1999). EGFR activation mediated by ANGII-AT_1R binding leads to synthesis of transforming growth factor β (TGF β) and fibronectin (Eguchi et al. 1998). ANGII is also implicated in the upregulation of oxidized low density lipoprotein receptor, LOX1R, which may suggest a role for AT_1R in the progression of atherosclerosis (Li et al. 1999). AT_1R activates many signaling pathways that make it an intriguing target for therapy.

1.1.3. AT_1R Regulation

In the presence of ANGII, AT_1R will undergo internalization. Once internalized, AT_1R may be degraded in lysosomes or returned to the plasma membrane (Fig 3). Internalization of AT_1R has been shown to be dependent on β-arrestin and dynamin, both of which are markers for clathrin coated pits (Gaborik et al. 2001). Chronic stimulation of the receptor by its ligand will lead to a decrease in receptor responsiveness. Upon binding of ANGII, AT_1R undergoes a conformational change which is the substrate for phosphorylation by GPCR kinases (GRKs). Once phosphorylated; the receptor is bound by β-arrestin which prevents interaction with G proteins, leaving the receptor desensitized. The phosphorylated receptor is now a target for endocytosis via clathrin coated pits (Ferguson 2001) (Fig 3). The C-terminus has been shown to be essential for proper AT_1R internalization as receptors mutated to be lacking the C-terminus impairs ANGII induced endocytosis (Mukherjee et al. 1982; Hunyady et al. 1994; Thomas et al. 1995).

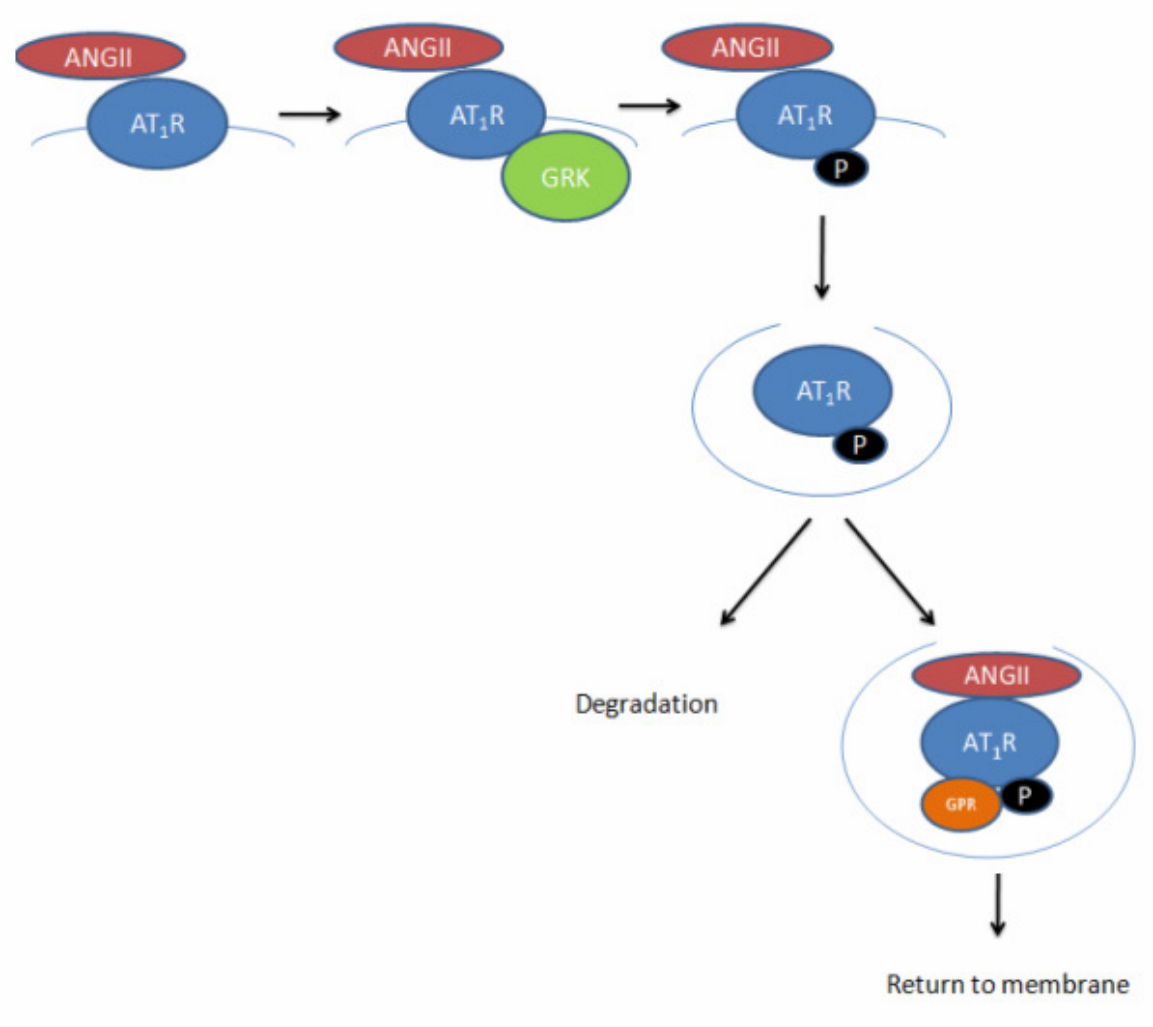

Figure 3: Schematic of ANGII-AT_1R binding. ANGII binding causes a conformational change in the receptor, which leads to phosphorylation of AT_1R. Once phosphorylated the receptor is targeted to be endocytosed in a clathrin coated pit. In the pit, the receptor can be degraded in a lysosome or recycled to the cell surface. GPCR specific phosphatases (GPR) dephosphorylate AT_1R which will lead the receptor back to the plasma membrane.

The vesicles in which GPCRs are endocytosed in response to ligand binding are enriched with GPCR specific phosphatases (GPR) (Ferguson 2001) (Fig 3). Should the cell require AT_1R to be returned to the plasma membrane, GPR would act on the receptor, dephosphorylating it, and the receptor is recycled. Rab4 and Rab11, small GTPases, have been shown to be involved in the recycling of AT_1R (Li et al. 2008) (Fig 3). GPCR recycling may take minutes while internalization occurs within seconds.

1.2 Animal Models

1.2.1 Nephrectomy Model

Renal mass reduction is a model used to study chronic kidney disease (CKD). Complications associated with CKD include: anaemia, hypertension, inflammation and sympathetic overactivation (Parmar 2002; Koomans et al. 2004; Kerr 2006; Garrido et al. 2009). Hypertension plays a key role in the progression of CKD and can lead to cardiovascular complications and death. In early stages after nephrectomy the RAS is thought to play a critical role in the development of hypertension in this model. Renal AT_1R have been shown to be involved in the development of hypertension in another model through Crowley et al's work with $AT_{1A}R$ knockout mice. These transgenic mice underwent kidney cross-transplantation surgeries and it was found that only the animals with kidney $AT_{1A}R$ expression experienced cardiac hypertrophy and hypertension when infused with exogenous ANGII (Crowley et al. 2006).

A 5/6 nephrectomy will lead to: elevated blood pressure, increased renal AT_1R expression and increased ANGII positive cells 8 weeks after surgery (Vaziri et al. 2007). The surgery for this animal model involves completely removing one kidney and

reducing the remnant kidney to 1/3 of its original size. This effect has been shown to be prolonged until 12 weeks post-surgery (Zhao et al. 2010). However after a longer time period post-surgery, it has been reported that AT_1R expression decreases 10 months after nephrectomy possibly due to downregulation caused by sustained activation by intrarenal ANGII (Sui et al. 2010). The renal AT_1R changes in animal models of renal failure are summarized in Table 1. Plasma ANGII levels are higher than controls at 2 weeks, but are subsequently normalized despite persistence of hypertension (Mackie et al. 2001). This observation suggests that circulating levels of ANGII are not the causative factor of sustained hypertension in this animal model (Mackie et al. 2001).

5/6 Nephrectomy is associated with LV hypertrophy (Kennedy et al. 2008; Sviglerova et al. 2010) . AT_1R is thought to play a role in hypertrophy because of the beneficial effect of AT_1R blockade (Liu et al. 2004). The increase in LV size has implications for ejection fraction (EF); a change which is thought to be transient: starting with an initial unchanged EF, then increase, followed by eventual decrease (Toblli et al. 2008). Understanding the RAS involvement in CKD will advance the development of therapies.

CKD is defined as a decrease in glomerular filtration rate (GFR) and kidney damage (Fukai et al. 1999; Ito 2011). In early stages of CKD, GFR is maintained or even higher than normal due to increased glomerular pressure in attempt to compensate for the loss of nephrons. However, this increased pressure and filtration rate cannot be maintained and eventually leads to a decrease in GFR and therefore function of the kidney (Chamberlain et al. 2007).

Table 1: Summary of changes in renal AT_1R in animal models of renal failure.*

Year	Animal	Surgery	Timeline	Renal AT_1R change	Method	Reference
1997	Sprague Dawley Rats	Unilateral Nx	1 week	No change	^{125}I-[Sar^1, Ile^8]ANGII binding assay	(Valentin et al. 1997)
1999	Sprague Dawley Rats	2K1C	1 week	--	RT-PCR	(Wang et al. 1999)
2002	Sprague Dawley Rats	Subtotal Nx	4 week	--	^{125}I-[Sar^1, Ile^8]ANGII binding assay	(Cao et al. 2002)
2005	Wistar Rats	5/6 Nx	12 week	--	RT-PCR	(Joly et al. 2005)
2007	Sprague Dawley Rats	5/6 Nx	8 week	++	Western blot	(Vaziri et al. 2007)
2010	Sprague Dawley Rats	Unilateral Nx	10month	--	Western blot	(Sui et al. 2010)
2010	Wistar Rats	5/6 Nx	12 week	++	Western blot	(Zhao et al. 2010)

*Subtotal Nx refers to removing one kidney, then ligating the 2 of 3 renal arteries of the remnant kidney, no part of the kidney is excised. 2Kidney 1 Clip (2K1C) 1 kidney has its renal arteries completed occluded.

By 8 weeks after surgery, this animal model represents a stage of CKD characterized with diminished GFR (Chamberlain et al. 2007), renal fibrosis (Piecha et al. 2008), increased proteinuria (Vaziri et al. 2007), lowered creatine clearance (Vaziri et al. 2007), hypertension (Vaziri et al. 2007) and LV hypertrophy (Moriguchi et al. 2011). While cardiac fibrosis is associated with end stage renal disease (ESRD), this time point does not produce myocardial fibrosis (Moriguchi et al. 2011). The 8 week time point was chosen as papers studying AT_1R following 5/6 Nephrectomy found changes in renal AT_1R between 4-12 weeks (Cao et al. 2002; Zhao et al. 2010; Vaziri et al. 2007; Joly et al. 2005).

1.2.2. Myocardial Infarction

Ligation of the LAD artery will contribute to damage to the heart leading to myocardial infarct (MI), neurohormonal impairment and decrease myocardial blood flow (MBF). In response to MI induced by coronary artery ligation, nonmyocytes expressed a drastic increase in cardiac AT_1R expression at one week post-MI (Lefroy et al. 1996). The increase was localized in the infarcted areas that were infiltrated by fibroblasts and showed significant collagen deposition. Myocyte AT_1R expression was also upregulated, however to a lesser extent (Meggs et al. 1993). The literature consistently shows an increase in AT_1R expression in the heart, both myocyte and nonmyocytes in this animal model (Meggs et al. 1993; Lefroy et al. 1996; Makino et al. 1996; Tan et al. 2004). A small decrease in receptor binding was reported post-MI in the renal tissue of rats with large (greater than 30%) infarct (Tan et al. 2004). Statistically insignificant changes were observed in kidneys of animals with a small infarct (Tan et al. 2004). AT_1R changes post-

LAD ligation are summarized in Table 2. Cardiac and plasma ANGII levels increase within the first day after LAD ligation inducing MI, however expression levels normalized by 4 weeks post-MI (Leenen et al. 1999). MI will eventually lead to heart failure; which is characterized by diminished LV function (Dixon et al. 1990).

1.2.3. Reperfused Myocardial Infarction

Transient ligation of the LAD followed by reperfusion has previously been used to study ischemia reperfusion injury (Ikeda et al. 2006; Higuchi et al. 2008). Higuchi et. al used [^{11}C]KR31173, an AT_1R PET radioligand, to study changes in LV AT_1R after transient ligation-reperfusion (Higuchi et al. 2010). The LAD of male Wistar rats was occluded for 20-25 minutes then released. Autoradiography studies showed increased [^{125}I]-[Sar^{1}Ile^8]ANGII binding in LAD territory 1 week and 3 weeks post-surgery while non infarcted control rats showed no change in labelled ANGII binding (Higuchi et al. 2010) Elevated AT_1R binding was observed until 3 months post-surgery. *In vivo* PET images showed uptake ratio of infarct to remote areas was 2.2±0.9, similar to that of the autoradiography results (Higuchi et al. 2010). The number of animals used in the PET study was small (n=3) and the authors describe the successful cardiac PET scans as a proof of concept and a launching point for further cardiac studies.

1.3 MicroPET

PET is a non-invasive *in vivo* imaging technique. This technology is currently used in the clinical setting as a diagnostic tool in diseases such as cancer (to detect tumours) and cardiac disease (to measure blood flow and glucose uptake). PET imaging is the

Table 2: Summary of changes in AT_1R post-LAD ligation (transient and permanent)

Year	Animal	Surgery	Timeline	LV AT_1R change	Renal AT_1R change	Method	Reference
1993	Sprague Dawley Rats	LAD ligation	1 week	++	NA	^{125}I-[Sar^1, Ile^8]ANGII binding assay	(Meggs et al. 1993)
1996	Sprague Dawley Rats	LAD ligation	1 week	++	NA	^{125}I-[Sar^1, Ile^8]ANGII binding assay	(Lefroy et al. 1996)
2004	Wistar Rats	LAD ligation	4 week + 8 week	++	-	^{125}I-[Sar^1, Ile^8]ANGII binding assay	(Tan et al. 2004)
2010	Sprague Dawley Rats	20minute LAD ligation	1 week + 3 week	++	NA	^{125}I-[Sar^1, Ile^8]ANGII binding assay	(Higuchi et al.)
2010	Sprague Dawley Rats	20minute LAD ligation	1 week	++	NA	[^{11}C]KR31173 PET imaging	(Higuchi et al.)

most sensitive of the available non-invasive imaging modalities. The half lives of the isotopes are short and an onsite cyclotron and complex radiochemistry may be required.

A labeled compound, known as a tracer, is injected into the subject, and decays releasing a positron. After traveling a short distance, this positron will interact with an electron in the surrounding area. The positron and electron will annihilate each other, releasing two gamma rays of 511keV that travel in opposite directions. The two gamma rays emitted are captured by detectors at 180^{o} from each other (Fig 4).

Using a small animal PET scanner in experimental research minimizes the number of animals needed for the experiment because an animal does not need to be sacrificed before examination. This allows the animal to serve as its own control as it can be scanned several times over the course of the experiment.

Tracers with higher specific activity (high amount of radioactivity/amount of tracer mass) will allow us to detect low concentrations of receptors. Low specific activity implies that more of the injected mass is unlabelled tracer which will bind to the receptor of interest but cannot be detected by the PET scanner. The tracer is used in small doses to avoid any physiological effect and according to Jagoda et al receptor saturation should be below 5% (Jagoda et al. 2004).

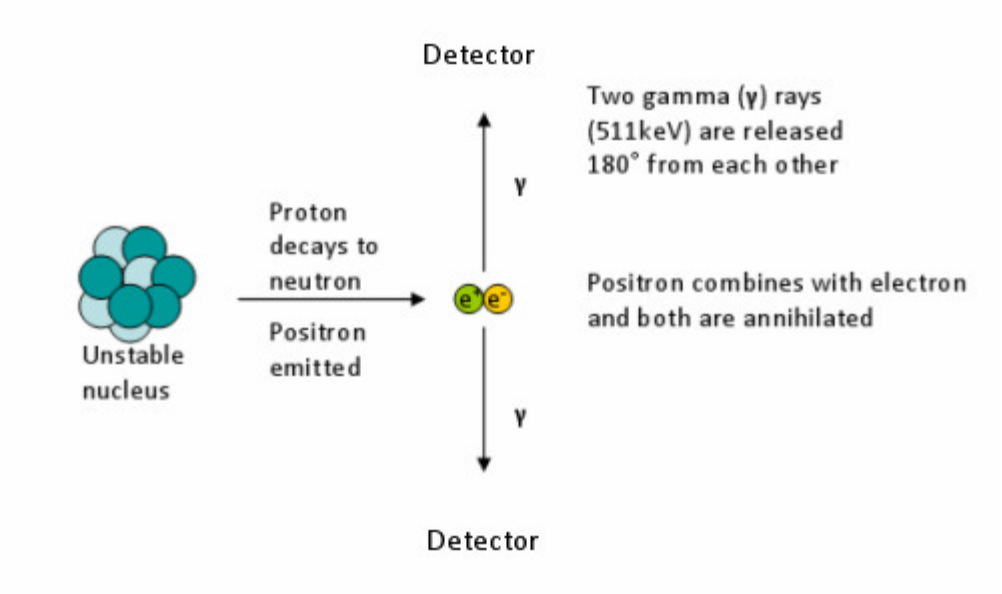

Figure 4: Diagram of Positron Emission Tomography Concept. A positron is emitted from the unstable radiotracer. When the positron interacts with an electron in the surrounding environment both are annihilated. Two gamma (γ) rays are produced in this interaction and are released 180° of each other. The γ rays are detected simultaneously in an external detector.

1.3.1. [^{13}N]Ammonia

[^{13}N]Ammonia is a PET radiotracer used in quantification of regional myocardial perfusion due to its high myocardial retention and rapid clearance from the blood pool (Shah et al. 1985). Scanning the animals with [^{13}N]ammonia will indicate perfusion in the tissue of interest.

1.3.2. O-[^{11}C]Methyl-Candesartan

O-[^{11}C]Methyl-candesartan is a radiotracer used to image AT_1R developed in our laboratory (Fig 5). The parent compound for this tracer is the anti-hypertensive drug, Candesartan (Nishikawa et al. 1997). [^{11}C]Methyl-candesartan is produced with >99% radiochemical purity, >90% chemical purity and in 50-70% yield (Hadizad et al. 2009). The IC_{50} of Candesartan is 66nM is similar to the IC_{50} of O-methyl-candesartan which is 110nM (Kubo et al. 1993). The diminished affinity of the methyl ester derivative of candesartan is explained by the alteration of the carboxyl group of the parent compound. The tetrazole moiety and carboxyl group of candesartan are involved in binding to Arg^{167} (TMV) and Lys^{199} (TMIV) of AT_1R respectively (Vauquelin et al. 2001). As seen in Fig 5, the carboxyl group is converted to an ester in the methylated form which would alter the interaction with Lys^{199} thereby reducing the affinity of O-methyl-candesartan compared to its parent compound, candesartan.

Ex vivo time course and biodistribution studies were previously performed on male Sprague-Dawley rats using [^{11}C]methyl-candesartan (Hadizad et al. 2009).

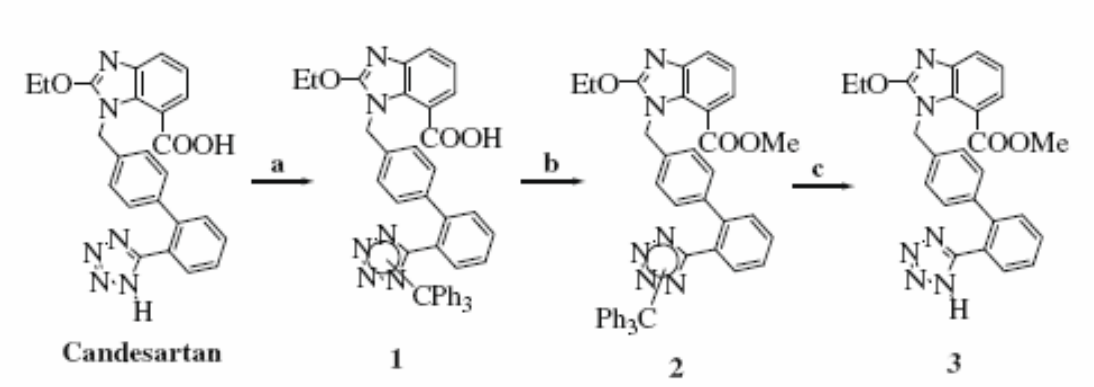

Figure 5: Synthesis schematic of [^{11}C]methyl-candesartan. Reagents and conditions: (a) TEA, trityl chloride, CH2Cl2; (b) Methyl Iodide, K_2CO_3, DMF, room temperature, 15 min; (c) HCl (1 N), DMF, 65–70°C, 1 h; (d) HCl (1 N), DMF, 90°C, 1.5 h (Hadizad et al. 2009).

In competition experiments, rats were coadministered or preinjected with AT_1R blockers (ARBs) (candesartan and losartan), AT_2R blocker (PD123,319), ANG(1-7) Mas receptor blocker (A-779), β-adrenergic receptor blocker (propranolol), or α_2-adrenergic receptor blocker (yohimbine). Rats treated with ARBs showed dose dependent decrease in tracer uptake in renal cortex and renal outer medulla while the other treatments did not affect tracer uptake. PET images using this tracer were performed in our group with promising results (Kirkpatrick et al. 2009). High contrast renal images and binding selectivity of the tracer led us to use [^{11}C]methyl-candesartan for further PET studies of animal disease models.

1.3.3. [^{11}C]Methyl-Candesartan Quantification

Tracer quantification for reversibly bound compounds can be represented using a graphical method known as a Logan plot (Logan et al. 1990). In essence, tracer uptake in the tissue of interest is plotted against concentration in the plasma at equilibrium. The mathematical representation of this is as follows:

$$ {}_0\int^T C_{PET}(t)dt/C_{PET}(T)\ (min) \qquad {}_0\int^T C_P(t)dt/\ C_{PET}(T)\ (min\cdot cm^3/ml) $$

Where $C_{PET}(t)$ represents the concentration in the tissue and $C_P(t)$ is tracer concentration in plasma which are plotted against each other in a Logan plot. A straight line is fitted to the linear section of this graph. The slope of this straight line corresponds to the distribution volume (DV) (ml/g) of the tracer. In terms of physiological studies, DV values can be used as an indirect indicator of protein or receptor expression. Tracer accumulation increase or reduction would suggest the molecule of interest that the tracer is binding to undergoes the same changes.

1.3.4. Partial Volume Effect

A PET scan produces a three dimensional (3-D) representation of the scanned subject. This 3-D image is composed of voxels, which are the smallest box shaped parts of the entire scan. PET tracers emit radioactivity which is measured as activity within each voxel. A voxel with high activity means a high amount of PET tracer is present in that voxel. When analyzing the activity within a region of interest (ROI), we are in fact measuring the sum of the activity within all voxels which compose the ROI. Due to the limited resolution of the PET scanner (1.2mm), the voxels do not exactly correspond to the shape of the tissue of interest. To clarify, the voxels are not small enough to follow the exact contours of the tissue. The PET image produced from the scan is blurred to smooth the outline of radiotracer distribution. This blurring leads to part of the signal in a given voxel spilling out and being measured outside of the actual source. The limited resolution and 3-D blurring will cause a partial volume loss effect (PVE) which leads to measured activity in PET images to be underestimated from actual activity.

While all PET images will have partial volume losses, in terms of comparison it is only a concern when the tissue of interest varies in size as this will affect the degree of PVE. The more voxels included in an ROI will lead to less of an underestimation of true activity than an ROI with fewer voxels. In terms of this study, nephrectomy will cause a change in the remnant kidney size that will affect [^{11}C]methyl-candesartan distribution and analysis. The remnant kidney ROI in the nephrectomized group will have more voxels than the control kidney, suggesting that control kidney ROI analysis will lead to a greater underestimation of activity. Therefore it is essential to determine a correction method to

account for the varying kidney sizes of the nephrectomy animal model to make comparison possible.

1.3.5. Other Radiotracers for *In Vivo* Imaging of AT_1R

AT_1R tracer development started in 1995 with the production of [^{11}C]MK-996 (Mathews et al. 1995). Due to difficulty of tracer synthesis, further reports were not published and [^{11}C]L-159,884 was developed by the same group (Mathews et al. 2004). PET imaging using [^{11}C]L-159,884 was performed in Beagle dogs and a baboon showing specificity for renal AT_1R (Szabo et al. 1998). However, upon comparison with [^{11}C]KR31173, another AT_1R tracer, it was found that [^{11}C]KR31173 showed higher specificity (Zober et al. 2006).

Xia et al used [^{11}C]KR31173 to study a porcine disease model of renovascular hypertension (RVH) to investigate changes in renal AT_1R (Xia et al. 2008). While tracer uptake was decreased because of reduced blood flow to the kidney, binding was increased in the stenotic kidney. The increased binding of [^{11}C]KR31173 *in vivo* PET studies were corroborated with [^{125}I]-[Sar^{1}Ile^8]ANGII autoradiography, which showed significant correlation between *in vivo* and *in vitro* binding of AT_1R in renal cortex (Xia et al. 2008).

A preliminary study (presented in abstract form) was performed in four healthy human subjects who were scanned with [^{11}C]KR31173 (Bravo et al. 2011). Twenty four hours later, two subjects were pretreated with Olmesartan, an ARB, and then scanned again. Pretreatment with Olmesartan led to a 51% decrease in myocardial [^{11}C]KR31173 retention (Bravo et al. 2011). This report is the only AT_1R PET radiotracer study involving human subjects.

[^{11}C]TH4 is the desethyl derivative of [^{11}C]methyl-candesartan and was also synthesized by Hadizad et al, however its use is limited to *ex vivo* analysis (Hadizad et al. 2009). Male Sprague Dawley rats were used in biodistribution competition studies using the ARBs, AT_2R blocker, ANG (1-7) Mas receptor blocker, β-adrenergic receptor blocker, and α_2-adrenergic receptor blocker as in the [^{11}C]methyl-candesartan competition studies. It was observed that AT_1R blockade reduced [^{11}C]TH4 uptake but not to the extent of [^{11}C]methyl-candesartan uptake. [^{11}C]TH4 uptake was also reduced by the Mas receptor blockade, suggesting that the radiotracer was not selective of AT_1R over Mas receptor. Because of the reduced selectivity of [^{11}C]TH4, it was determined that [^{11}C]methyl-candesartan would be a more appropriate renal AT_1R imaging agent.

[^{11}C]Methyl-losartan, another AT_1R tracer developed by our group, is the ^{11}C-methyl derivative of the ARB, losartan (Hadizad et al. 2011 (In Press)). PET images showed highest uptake in kidney cortex, kidney medulla and liver. ARB treatment reduced tracer uptake in renal cortex and medulla by 74-86% (Antoun et al. 2010). This decrease was not seen in animals treated with AT_2R or Mas receptor blockade. The *in vivo* PET data was presented as an abstract and further evaluation and synthesis optimization studies are ongoing (Antoun et al. 2010).

Finally, a Single Photon Emission Computed Tomography (SPECT) tracer, ^{99m}Tc Losartan, was used to monitor AT_1R changes in mice following LAD ligation. SPECT imaging uses radiotracers that are labelled with gamma ray emitting isotopes. As the radiotracer decays, the gamma rays are detected externally by a gamma camera. Tracer uptake per gram of cardiac tissue was significantly higher in infarcted hearts, when compared to

control hearts at 3 weeks post-surgery (Verjans et al. 2008). Within the MI hearts, uptake in the infarct zone was 2.4 times higher compared to remote regions (Verjans et al. 2008).

AT_1R imaging has potential to revolutionize treatment of cardiovascular diseases. The amount of interest in this field reflects the need for effective AT_1R imaging agents. Only one AT_1R tracer, [^{11}C]KR31173, has been used in humans which underlines the importance of translating *in vivo* animal imaging to the clinical setting.

2. Clinical Significance

Using a non invasive imaging technique, predicting response to RAS blockade treatment will be possible. Angiotensin Converting Enzyme inhibitors (ACEi) and ARBs have been shown to inhibit cardiac hypertrophy, glomerulosclerosis and to lower blood pressure in animal models of renal failure and in humans. Heart failure is also commonly treated with RAS blockade which has displayed beneficial effects in limiting cardiac remodeling and preserving LV function. While RAS blockade is a common method of therapy of cardiovascular disease, it is not effective in all patients. Even those that experience beneficial effects of this medication do not experience complete reversal of disease state. This underlines the need for better understanding of mechanistic progression of cardiac and renal disease. There is no method to reliably predict efficacy of these ARBs and ACEi's in patients which limits the efficiency of therapy. The transient LAD ligation followed by reperfusion provides a representative animal model of MI patients who undergo an angioplasty. Being able to guide medication non-invasively with PET will facilitate therapy in case AT_1R levels are not affected in particular patients. Imaging the AT_1R will allow for identification of receptor expression abnormalities in patients, understanding the contribution of the AT_1R to the progression of disease and will make therapy truly individualized.

3. Rationale, Research Aims, Hypotheses and Objectives

3.1 Rationale

The rationale for this project is based on the following:

1) Animal models of CKD show upregulation in renal AT_1R expression 8-12 weeks post-5/6 subtotal nephrectomy (Vaziri et al. 2007)
2) One and 4 weeks post-LAD ligation, animal models exhibit upregulation in cardiac AT_1R and downregulation in renal AT_1R, respectively (Tan et al 2004; Lefroy et al. 1996; Higuchi et al 2010)
3) Treatments blocking the RAS, such as ARBs and ACEi, have shown beneficial effects in hypertension, heart failure and renal failure patients (Pfeffer et al. 1992; Makino et al. 1996; Hall et al. 1997; Cohn et al. 2001; Maggioni et al. 2002); (Barreras et al. 2003; McMurray et al. 2003)
4) *In vivo* imaging has displayed an upregulation in cardiac AT_1R in post-LAD ligation which peaks between 1 and 3 weeks following surgery (Verjans et al. 2008; Higuchi et al. 2010)

3.2. Research Aims

The overall aim of my project is to use non-invasive µPET scanning to measure temporal AT_1R changes in post-nephrectomized and MI rats. We hope to translate [^{11}C]methyl-candesartan PET imaging to clinical use in humans and monitor response to treatment.

3.3. Hypotheses

3.3.1. Nephrectomized Rats:

Nephrectomized rats will exhibit preserved LV function, normal plasma ANGII levels, increased MBF, unchanged renal blood flow (RBF) and elevated kidney AT_1R.

8 weeks after nephrectomy:

1. [^{13}N]Ammonia will find an increase in MBF and no change in RBF
2. [^{11}C]Methyl-candesartan will measure an increase in kidney AT_1R expression
3. Partial volume loss correction (40-80 method) will be applied to nephrectomized and sham animals to provide a more accurate measure of [^{11}C]methyl-candesartan distribution in renal tissue
4. Western blot analysis will corroborate *in vivo* [^{11}C]methyl-candesartan μPET findings

3.3.2. Ligation/Reperfusion Rats:

Post-LAD ligation rats will exhibit reduced LV function (MI), preserved LV function (transient LAD ligation), normal plasma ANGII levels, decreased MBF (MI), increase in cardiac AT_1R expression, and normal renal AT_1R expression. 2 weeks post-surgery:

1. [^{13}N]Ammonia will measure a decrease in MBF in 20min and permanent ligation groups
2. [^{11}C]Methyl-candesartan will detect no change in renal AT_1R expression post-LAD ligation
3. [^{11}C]Methyl-candesartan will detect an increase in cardiac AT_1R expression after transient 20min LAD ligation
4. Western blots will corroborate *in vivo* [^{11}C]methyl-candesartan μPET findings

3.4. Specific Objectives:

1. Use echocardiography to assess LV function
2. Measure plasma ANGII peptide levels in control and experimental animals using an EIA kit
3. Use [^{13}N]ammonia μPET to image MBF *in vivo* in control, nephrectomized and LAD ligated animal groups
4. Use [^{11}C]methyl-candesartan μPET tracer to image renal AT_1R expression *in vivo* in control and post-nephrectomy animal model
5. Use [^{11}C]methyl-candesartan μPET tracer to image cardiac and renal AT_1R expression *in vivo* in control, post-MI and reperfused ligation animal model
6. Use 40-80 method to correct for PVE in nephrectomized and sham animals
7. Conduct Western blot to corroborate μPET findings

4. Methods

All in vitro work, PET and echo data analysis was performed by me.

See Fig 6 for timeline of experiments and Fig 7 for n values for each protocol.

4.1. Nephrectomy Model

A 5/6 nephrectomy involves removing the entire right kidney and 2/3 of the left kidney (Vaziri et al. 2007; Sui et al. 2010) (Fig 8A). The surgery was completed in two sittings, one week apart to increase survival rate. Male Sprague Dawley rats were anesthetized with 2 ml/min isoflurane. A dorsal midline incision on the right side was made and the abdominal cavity was entered. Surrounding tissue was removed from the right kidney, the adrenal gland separated and the renal blood vessels and ureter were ligated. The kidney was then removed from the abdominal cavity by transecting the vessels and ureter distal to the ligated spot. The incision was closed and the animal was allowed to heal for one week. For the next stage the animal was anesthetised as before. A dorsal midline incision was made into the abdomen; the intestine was retracted to the side to expose the left kidney. The left kidney was freed from connective tissue. A suture was placed around each pole of the kidney at the 1/3 position. The sutures were ligated and 1/3 kidney on each end was excised beyond sutures. The incision was closed with suture and stapled. Buprenorphine was administered twice daily by subcutaneous injection for post-operative analgesia.

Sham animals were prepared as described above. However kidneys were exposed then placed back into the abdominal cavity unaltered. Sham animals underwent 2

surgeries one week apart to simulate nephrectomy conditions. The sham animals received the same analgesic medication.

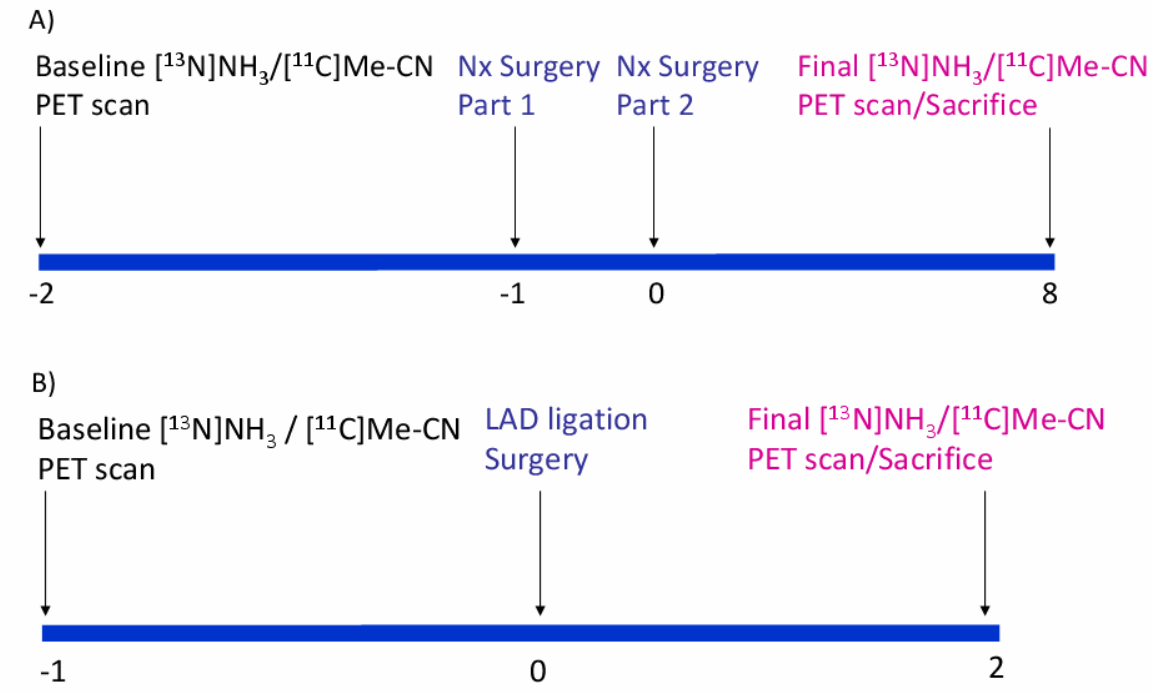

Figure 6: Timeline in weeks for experiments. A) Nx protocol and B) Ligation/Reperfusion protocol.

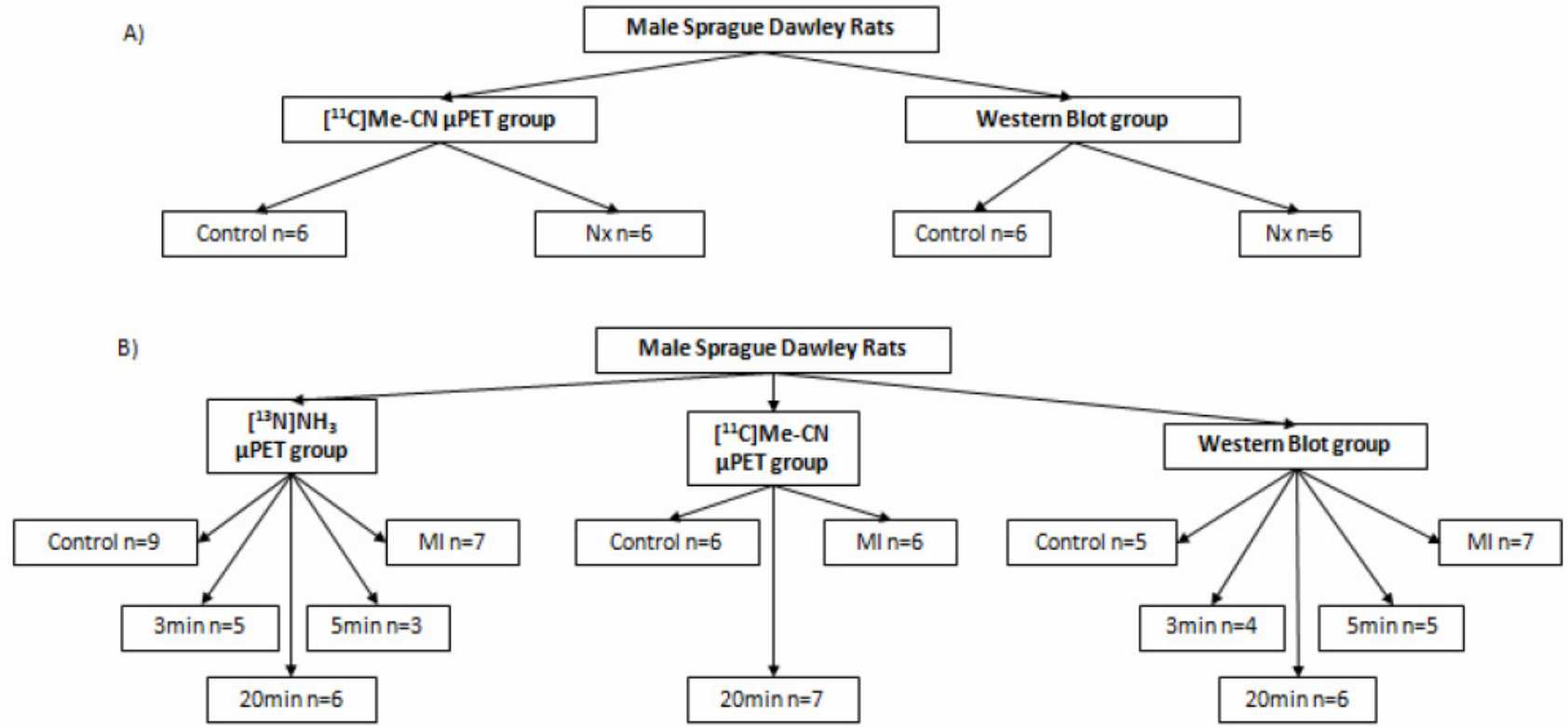

Figure 7: N values of A) Nx protocol and B) Ligation/Reperfusion protocol.

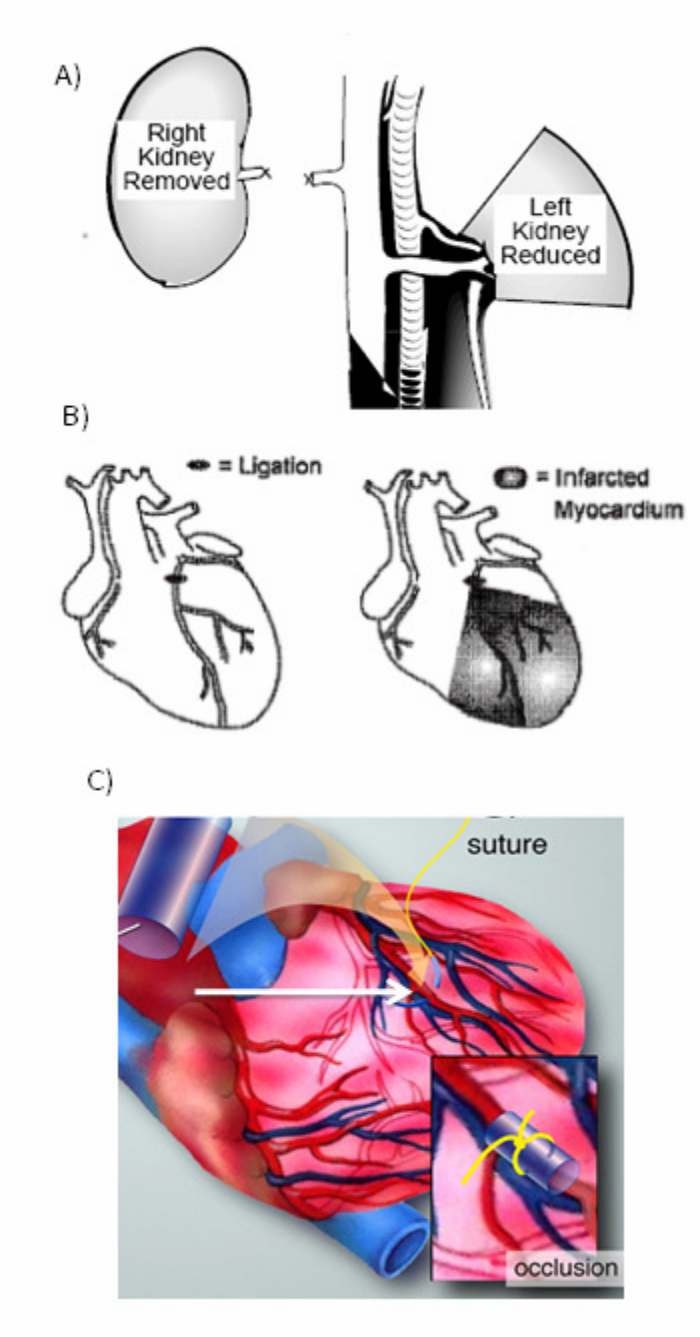

Figure 8: A) 5/6 Nx surgery diagram. RK is removed in its entirety, one week later, inferior and superior poles of LK are ligated and excised B) Permanent LAD ligation surgery diagram. LAD is ligated at proximal end of artery. LV distal to ligation will be infarcted (Suuronen et al. 2007) C) Ligation/Reperfusion surgery diagram. White arrow points to LAD. Plastic tubing is placed over LAD and suture is ligated around artery and tubing for 3, 5, or 20minutes then released (Klocke et al. 2007).

4.2. Left Anterior Descending Coronary Artery Ligation-Myocardial Infarct Animal Model

To induce an ischemic insult to the myocardium, a surgical ligation of the LAD coronary artery was performed in rats (Meggs et al. 1993; Lefroy et al. 1996; Makino et al. 1996; Leenen et al. 1999; Tan et al. 2004; Suuronen et al. 2007) (Fig 8B). Male Sprague Dawley rats were anesthetized with 2 ml/min isoflurane, intubated and attached to a ventilator. A cranio-caudal incision was made on the chest and pectoral muscles blunt dissected apart, exposing the rib cage. Muscles of the third or fourth intercostals space were dissected and ribs held apart by retractors. Thymus was retracted out of the way and the pulmonary trunk and the left atria located. Silk suture (5-0) was driven using a small curved needle under the LAD and the ligature tied. Ribs were stitched together using suture (3-0) and the air gently squeezed out of the thoracic cavity. Pectoral muscles were re-positioned and the wound closed by staples. Animals were resuscitated using ventilation with high oxygen. Buprenorphine was administered twice daily by subcutaneous injection for post-operative analgesia.

Sham animals underwent similar anesthetic and intubation procedures. The heart was exposed in the same manner as described as above, however the heart muscle was left untouched then placed back into the thoracic cavity. The sham animals received the same analgesic medication.

4.3. Model of Reperfused Myocardial Infarction

To introduce a temporary occlusion of the LAD blood flow, a surgical procedure was performed similar to the permanent LAD ligation described above (Ikeda et al. 2006; Higuchi et al. 2008; Higuchi et al. 2010). A polypropylene (PE50) tube was placed between the suture and the vessel for safer removal of occlusion (Fig 8C). Instead of tying off the LAD permanently, the ligated animal remained on the ventilator for 3, 5 or 20min, at which point the suture was loosened and blood flow re-established.

4.4. Echocardiography

Echocardiography was used to determine LV dimensions and to evaluate cardiac function, particularly important in evaluation of post-MI rats developing heart failure. Measurements obtained include: LV end diastolic diameter (EDD), LV end systolic diameter (ESD), interventricular septal thickness (IVS) and posterior wall thickness (PWT). Measured dimensions will be used to calculate the EF and fractional shortening (FS).

Cardiac function was evaluated using a ViewSonics Vevo 770 High-resolution imaging system. Briefly, male Sprague Dawley rats were anesthetized with isoflurane (1-2%) and hair removed from the imaged area. Parasternal long axis and short axis views were recorded in B- and M-mode, with the motion of the cardiac walls recorded by summation across several cycles (Cherin et al. 2006). 716B scanhead was used, at the transducer frequency of 23.5 MHz, with focal length of 17.5 mm and a field of view of 32 mm. M-mode recordings were used to visually confirm the presence of the infarct and

observe the wall motion abnormality. B-mode cine loops were used to delineate the shape of the LV at systole and diastole and calculate the volume.

4.5. Enzyme Immunoassay Kit

Plasma ANGII levels were determined with an ANGII EIA kit (Phoenix Pharmaceuticals) (Aoyagi et al. 2008). The immunoplate in the kit is pre-coated with the secondary antibody and non-specific binding sites are blocked. The primary ANGII antibody will bind to the secondary antibody and the biotinylated peptide and peptide in the samples will competitively bind to the primary antibody. The biotinylated peptide interacts with streptavidin-horseradish peroxidase (SA-HRP) which will catalyze the substrate solution. The yellow colour produced at the end of the reaction is directly proportional to the amount of biotinylated peptide-SA-HRP complex but inversely proportional to the amount of ANGII in the standards or samples. Briefly, peptides in plasma were separated through a C-18 SEP Pak (Waters). Peptide standards, positive controls and samples were loaded into wells in duplicate. Primary antibody followed by biotinylated peptide was added to each well, except blank wells. The plate was incubated for 2hours at room temperature. Next, SA-HRP was added to each well and the plate was left to incubate for 1hour at room temperature. TMB (substrate solution) was added into each well and the plate was incubated again for 1hour at room temperature. Finally, 2N HCl was added into each well to stop the reaction. Absorbance was read at 450nm. Concentrations of ANGII were generated using SigmaPlot software.

4.6. MicroPET

The animals were anesthetized with 2ml/min isoflurane. Rats were scanned using a dedicated small animal μPET camera (Siemens Inveon^{TM}). [^{13}N]ammonia, to measure blood flow, doses ranged from 1.52-2.99mCi. Before the [^{13}N]ammonia scan, a 10 minute transmission scan (Co-67) was acquired to facilitate attenuation correction (Fig 9). [^{11}C]methyl-candesartan, to detect AT_1R expression, was injected into the tail vein. Injected dose was approximately 0.5mCi and ranged from 6.25E-4 to 1.08E-2μg/g. The [^{11}C]methyl-candesartan scans were 60 minutes in length and were preceded by a 30 minute [^{13}N]ammonia scan to delineate perfusion and 30 minute washout period (Fig 9). Data was reconstructed using Siemens Inveon Acquisition Workplace software. Dynamic histograms were created with the following frame composition: 12 x 10seconds, 3 x 60seconds and 11 x 300seconds.

4.7. Test-Retest Variability

Two users analyzed the same [^{11}C]methyl-candesartan images to compare DV values that were calculated using the 40-80 partial volume correction method. A Bland Altman plot was created to show variability between these users. To calculate interuser variability, test-retest variability (TRV) was used. The following equation comparing DV values was used to calculate TRV:

$$|\text{User 1} - \text{User 2}|/((\text{User 1} + \text{User 2})/2)$$

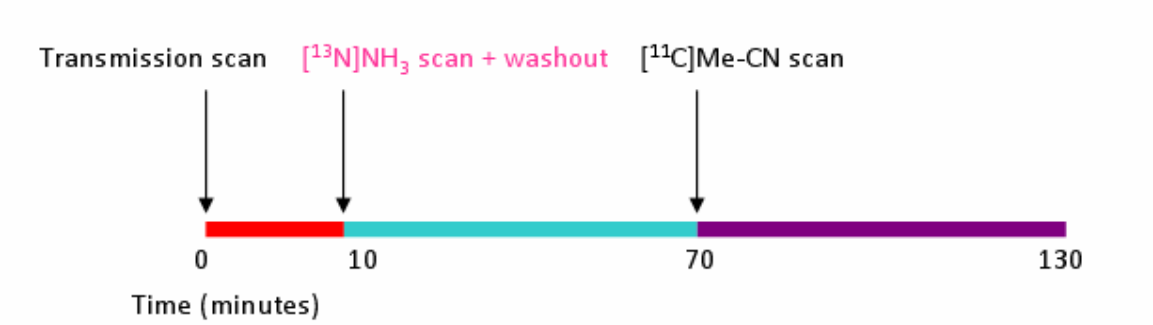

Figure 9: Timeline of [^{13}N]NH_3 and [^{11}C]methyl-candesartan PET scan. Ten minute transmission scan for attenuation correction, followed by [^{13}N]ammonia and activity washout period before scanning with [^{11}C]methyl-candesartan.

4.8. [^{13}N]Ammonia

4.8.1. [^{13}N]Ammonia Radiochemical Synthesis

[^{13}N]Ammonia was produced using standard clinical procedure.

4.8.2. [^{13}N]Ammonia μPET analysis

The Inveon Research Workplace (IRW) software was used to measure renal blood flow for nephrectomy protocol. PET scans were reconstructed such that only the first 2 minutes of the scan were included. The left atrium (LA) and kidney ROIs were drawn in early frames. Time activity curves and flow values (ml/g/min) were produced. The kinetic model used to calculate flow values was the one compartment model.

Myocardial perfusion analysis was performed using [^{13}N]ammonia PET scans analyzed using in house developed FlowQuant© software for cardiac perfusion (Klein et al. 2010). One compartment model was used and polar maps were generated for both animal models. For the ischemia/reperfusion study, cardiac perfusion analysis was conducted using the 17 segment model (Fig 10). This model was used to better regionalize blood flow defects within the LV. Segment 7, 8 and 12 represent the anterior surface of the LV, which was used as the area at risk. The anterior surface was chosen because this is the area of the LV that is normally supplied by the LAD. The lowest flow value in the area at risk was then compared as a ratio of the flow to the contralateral segment.

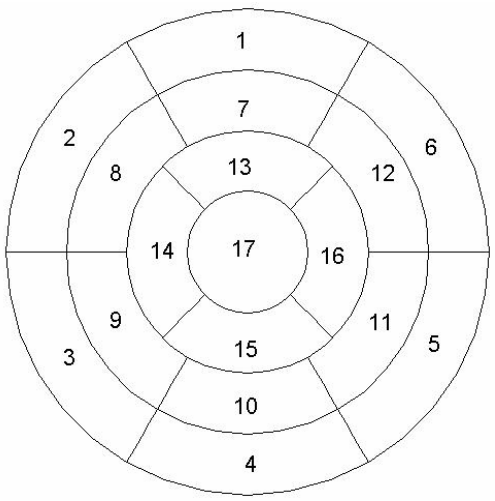

Figure 10: 17 Segment model of LV: Allows for regional description of LV blood flow deficiency when analysing [^{13}N]ammonia µPET scan.

4.9. [^{11}C]Methyl-Candesartan

4.9.1. [^{11}C]Methyl-Candesartan Radiochemical Synthesis

Synthesis of [^{11}C]methyl-candesartan is described by Hadizad et. al (Hadizad et al. 2009). It is a multistep process that begins with protection of the tetrazole group. Unlabeled candesartan was dissolved in an ice cooled solution of methylene chloride and triethylamine. Trityl chloride, the protecting group, was added to this solution. Reaction was raised to room temperature and left for 17hours. The tetrazole-protected candesartan was purified by flash column chromatography and used as the precursor for radiotracer production.

The isotope, ^{11}C, was produced by nuclear reaction $^{14}N(p,\alpha)^{11}C$ and reacted with O_2 in the cyclotron to produce [^{11}C]CO_2. From [^{11}C]CO_2, [^{11}C]CH_3 was produced in two ways: the gas method using the GE Healthcare TRACERlabT FX C Pro and the wet method. Using gas method, [^{11}C]CO_2 was converted to [^{11}C]CH_4 in the presence of a nickel catalyst in high heat conditions. [^{11}C]CH_4 was then converted to [^{11}C]CH_3I in the I_2 oven. Using the wet method, the [^{11}C]CO_2 is reduced by lithium aluminium hydride in tetrahydrafuran to produce [^{11}C]CH_3O^-. [^{11}C]CH_3O^- is then further reacted with phosphoric and hydriodic acid under high heat to produce [^{11}C]CH_3I.

The precursor and kryptofix were dissolved in dimethylformamide and added to potassium carbonate. [^{11}C]CH_3I was trapped in the reaction vessel and the temperature was raised to 65-70°C for 3minutes. Finally the radiolabelled tetrazole-protected tracer was deprotected using hydrochloric acid hydrolysis for 2min at 65-70°C.

4.9.2. [^{11}C]Methyl-Candesartan µPET Analysis

[^{11}C]Methyl-candesartan analysis was performed using Siemens IRW software. ROIs (Fig 11) were drawn around the LA at frame 3-5 and used as plasma input function. The ROI threshold was adjusted so that the LA ROI only included the voxels with the top 20% intensity.

Kidney ROIs were drawn at frame 17. The bottom 1/3 of the right kidney and bottom 2/3 of the left kidney was used for kidney ROIs. The top portions of the kidneys were avoided to reduce spillover effect from the liver. For nephrectomized rats, the remnant left kidney was used in its entirety because of its distance from the liver.

The colour scale was adjusted using a 20 step colour scale such that the kidney in question had one white dot (representing the highest voxel intensity). Then the lower limit of the colour was set to 50% of maximum intensity within the cube ROI. This 50% threshold was used to create the final kidney ROI. Liver ROIs were drawn in three different slices of the organ without any thresholding. From these ROIs, time activity curves and Logan plots were created. Plasma input correction was applied to DV calculated from the Logan plot analysis. From previous work, it was determined that the plasma to whole blood ratio of [^{11}C]methyl-candesartan is 1.58. Therefore all DV values were divided by this factor.

4.9.3. 40-80 Partial Volume Loss Correction Method

This method was used to correct for the different sizes of nephrectomized and sham kidneys. To account for the underestimation of activity measured by µPET, it

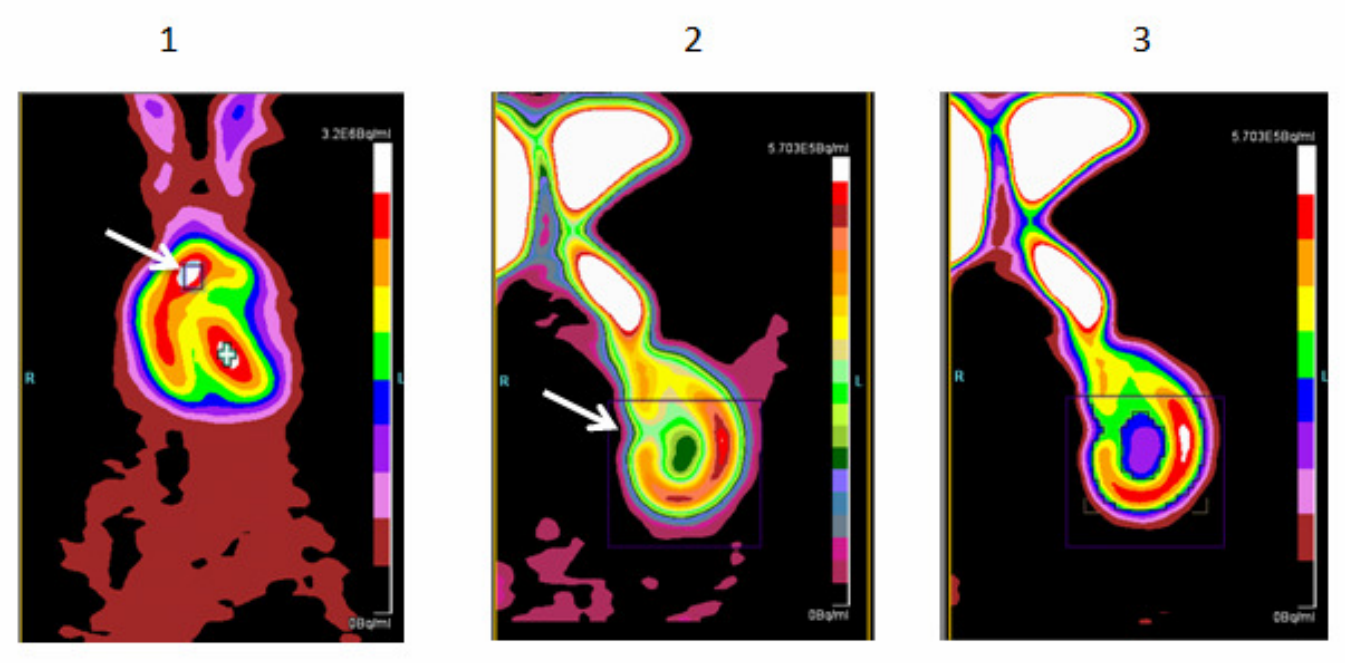

Figure 11: [^{11}C]Methyl-candesartan ROIs. Panel 1: Arrow points to LA. Sphere is drawn around LA and 20% highest voxels are included for LA blood input ROI. Panel 2: Arrow points to LK. Cube is drawn to encompass as much LK without liver interference. Panel 3: Cube drawn around LK threshold is set such that highest uptake voxels (50% cut off) are included in LK ROI.

has been determined that multiplying activity in an ROI drawn at 80% of maximum threshold by volume of an ROI drawn at 40% threshold will give a more accurate assessment of actual activity (unpublished data) (Fig 12). To implement this method for renal tissue µPET image analysis the LA and liver ROIs were drawn in the same manner as described above. The ROI method was altered for kidney analysis (Fig 13). For nephrectomized animals, a cube ROI was drawn around the entire left kidney. The maximum voxel intensity within the ROI was determined (available from the IRW software). From this maximum intensity, the 40% and 80% threshold were determined. To created the ROI at the 40% threshold ($ROI_{40\%}$), the value of 40% of the maximum intensity within the initial ROI was entered into the software. The $ROI_{80\%}$ was created in the same manner.

The ROIs for sham animals with whole kidneys were drawn differently. Because an ROI encompassing the whole kidney without interference from liver was impossible, only half of the kidney was used for the initial cube ROI. The hilus of the kidney was used as a landmark to indicate the half way point of the kidney.

The IRW software provides the following information needed for the 40-80 method: ROI volume, minimum, maximum and average intensity of activity. To determine actual activity in the kidney, volume of $ROI_{40\%}$ ($Vol_{40\%}$) was multiplied by the average voxel intensity of $ROI_{80\%}$ ($Avg_{80\%}$):

$$\textbf{Actual Intensity (Bq)} = \textbf{Vol}_{40\%} \times \textbf{Avg}_{80\%}$$

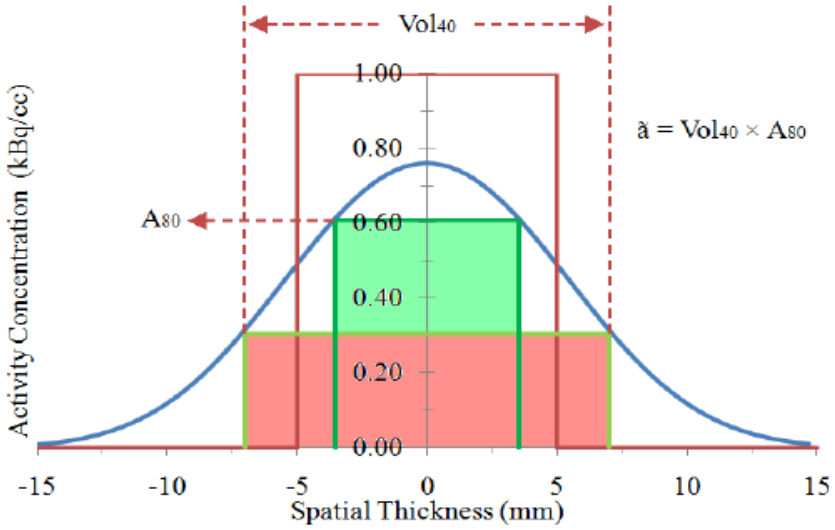

Figure 12: 40-80 Partial Volume Effect Correction Method. Red rectangle represents actual activity. Blue line represents underestimated activity measured with PET analysis. Activity in 80% threshold ROI (green rectangle, A_{80}) multiplied by area of 40% threshold ROI (red filled rectangle) represents actual activity (ã). This multiplication will correspond to actual activity represented by the area under the red outlined rectangle (Hunter, deKemp unpublished data).

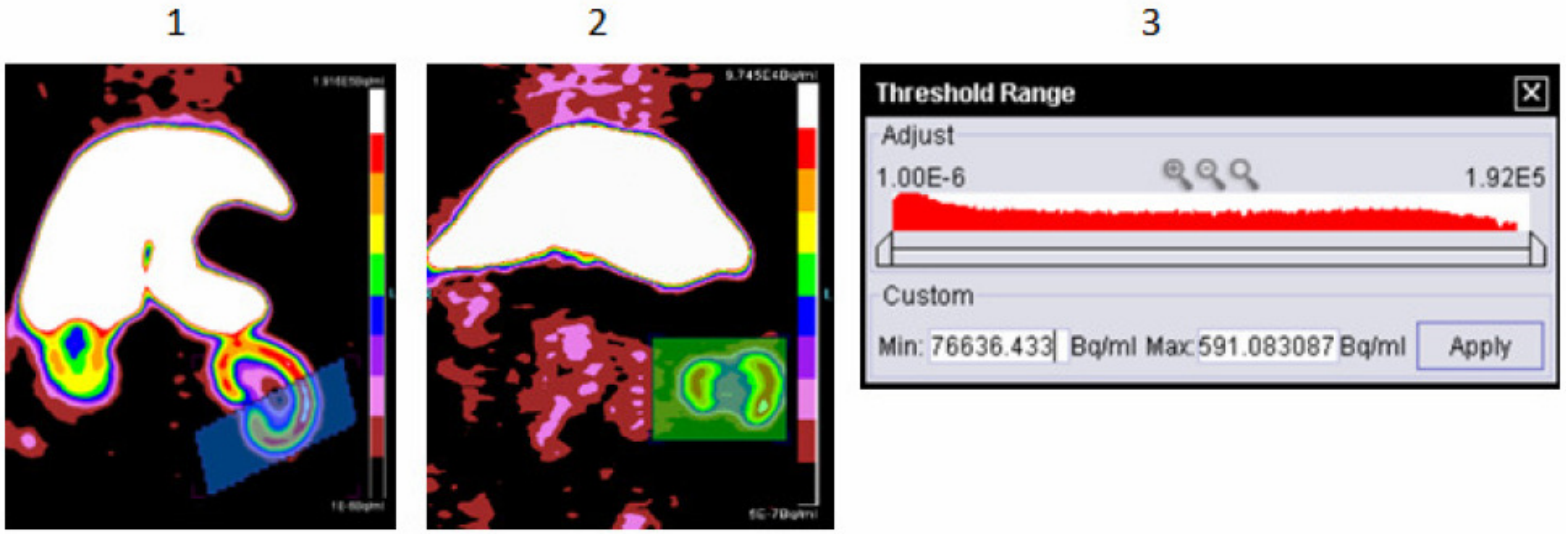

Figure 13: [^{11}C]Methyl-candesartan ROIs for 40-80 analysis. Panel 1: Half of intact LK included in cube ROI. Panel 2: Entire nephrectomized left kidney is included in ROI drawing. Panel 3: Limits of threshold can be calculated and manually inputted to create $ROI_{40\%}$ and $ROI_{80\%}$.

For sham animals, as mentioned only half of the kidney was included in the ROI. Therefore, one additional step for the sham group was to multiply the $Vol_{40\%}$ by 2 to represent the whole kidney.

To adjust DV values using the rationale of the 40-80 method, the following equation was used to correct DVs:

$$\textbf{Corrected DV} = [(DV_{80\%}/1.58) \times Vol_{40\%}]/\textbf{Kidney Weight}$$

Again, for the sham kidneys, $Vol_{40\%}$ was multiplied by 2.

4.10. Western Blot

To determine any changes in AT_1R protein expression Western blotting techniques were applied to cardiac and renal tissue homogenates and expression compared to control levels as previously described (Yoneda et al. 2005; Oestreicher et al. 2006). Western blot analysis techniques are based on the manufacturer's instructions (BioRad). Tissues of animals were rapidly excised and flash-frozen in liquid N_2. Heart and kidney were powdered and stored at -80°C until the time of the experiment. Powdered tissue was homogenized on ice using a polytron (2 × 15 sec) in lysis buffer (50 mM Tris·HCl, 150 mM NaCl, 1% Triton X100, pH 8) containing protease inhibitors (Complete protease inhibitor cocktail, Roche). Homogenate was centrifuged for 15min at 12000×g and supernatant collected. Protein concentration was determined using the BCA protein assay.

Resolving gel monomer solution (9.5%) was prepared by mixing deionized water (ddH_2O), 30% acrylamide, 1.5 M Tris, 10% SDS, 10% APS and TEMED and used with a stacking gel monomer. The electrophoresis tank was loaded with 1X electrophoresis

buffer (Tris, glycine, 10% SDS). Homogenized sample was diluted 1:2 in sample buffer (10% SDS, glycerol, 1 M Tris, dH_2O, 1% bromphenol blue), heated at 95°C for 3min and centrifuged for 1min. Supernatant was loaded onto the stacking gel, with 7 µl of molecular weight markers.

Electrophoresis was run at 150-180V until the tracking dye reached the bottom of the gel. Gel was removed and gently shaken in 1X transfer buffer (Tris, glycine) for 15min. The gel sandwich composed of filter papers, gel and membrane (polyvinylidene fluoride pre-soaked in 100% methanol and washed in ddH_2O) was assembled and immersed in the transfer tank filled with cold buffer, then run for two hours in a TransBlot cell with plate electrodes at 110V (4°C) with a 40W limit.

Membrane was removed, washed in 1X TBST for 5 min at room temperature and blocked for 1hour at room temperature in TBST with 10% skim milk. Membrane was incubated with the primary AT_1R rabbit polyclonal antibody (1:500) and 5% milk TBST for overnight at 4°C. Membrane was then washed 6 times with TBST (5min each wash) then incubated with secondary goat anti-rabbit antibody (1:5000) and 5% milk TBST for 45min at 4°C, and then washed 6 times with TBST (5min for each wash).

Membrane was washed with 1 mL of oxidizing agent, mixed with 1 mL of enhanced luminol reagent for 1 min and placed between two plastic sheets. Image was obtained using a CCD camera at an image station (FluorChem HD, Alpha Innotech, San Leandro, CA) connected to AlphaEase FC IS-9900 image analysis software (Alpha Innotech), adjusting the exposure time to optimize the contrast of the image. As a loading control, Glyceraldehyde 3-phosphate dehydrogenase (GAPDH) was also detected

using mouse GAPDH monoclonal antibody (1:5000) and donkey anti-mouse antibody (1:2000).

4.11. Biodistribution

Biodistribution study was used to confirm μPET findings for 5/6 nephrectomy animal model. Animals underwent 5/6 nephrectomy surgeries as described in 4.1. (both sham and nephrectomy). Eight weeks post-surgery, animals were injected intravenously with 1.5mCi of [^{11}C]methyl-candesartan (at time of first injection) and sacrificed by decapitation 15minutes following injection. The 15minute time point was decided based upon previous studies finding that at 15minutes is when kidney uptake was highest compared to blood tracer uptake (Hadizad et al. 2009). Tissues were dissected and placed in pre-weighed tubes. The radioactivity in these tubes was measured using a gamma counter. Activity was expressed as injected dose (%)(ID)/g then normalized to body weight.

4.12. Statistical Analysis

Results are presented as mean ± SD calculated as the average from data from each rat. Student's t-test was used to determine statistical significance, $p<0.05$ was considered significant. N values for each comparison are given in the text or in Figure/Table. Bland Altman plot and test-retest variability was used to compare inter-user variability for μPET analysis techniques.

5. Results

5.1. 5/6 Nephrectomy Model

5.1.1. Body and Organ Weights

At time of sacrifice, kidney and heart weights were measured. Hearts were left intact before weighing, and remnant kidneys were compared to whole kidneys in sham animals. No significant change in body weight was observed in sham and nephrectomized animals. However, as expected, when normalized to body weight, a significant increase was observed in both heart (21.4%) and kidney (29.3%) weights of nephrectomized animals when compared to shams (Table 3).

5.1.2. Echocardiography

Echocardiography was performed prior to final scan and sacrifice (8 weeks post-surgery). No changes were observed in EF of FS of nephrectomized and sham animals (Table 3).

5.1.3. Plasma ANGII

Plasma ANGII levels showed a trend to increase (38%) in nephrectomized animals when compared to sham animals (Fig 14). However, the n value used for this experiment was too low to make any statistically significant conclusions. Results using this kit have generally been unreliable and will be discussed in section 6.1.3.

5.1.4. [^{13}N]Ammonia µPET

MBF showed a 55% increase in nephrectomized animals when compared to sham animals 8 weeks post-surgery. RBF were similar between the two groups (Table 4).

Table 3: Body Weight, Heart Weight, Kidney Weight, Ejection Fraction and Fractional Shortening in Sham and Nx animals 8 weeks post-surgery

	Sham	Nx
n	10	6
Body Weight	579±57.3g	549±38.5g
Heart Weight/Body Weight	0.0026±0.02	0.0032±0.08*
Kidney Weight/Body Weight	0.0029±0.02	0.0037±0.05*
Ejection Fraction (%)	64.4±7.9%	62.7±7.5%
Fractional Shortening (%)	53.1±7.6%	55.1±7.5%

*$p<0.05$ compared to sham

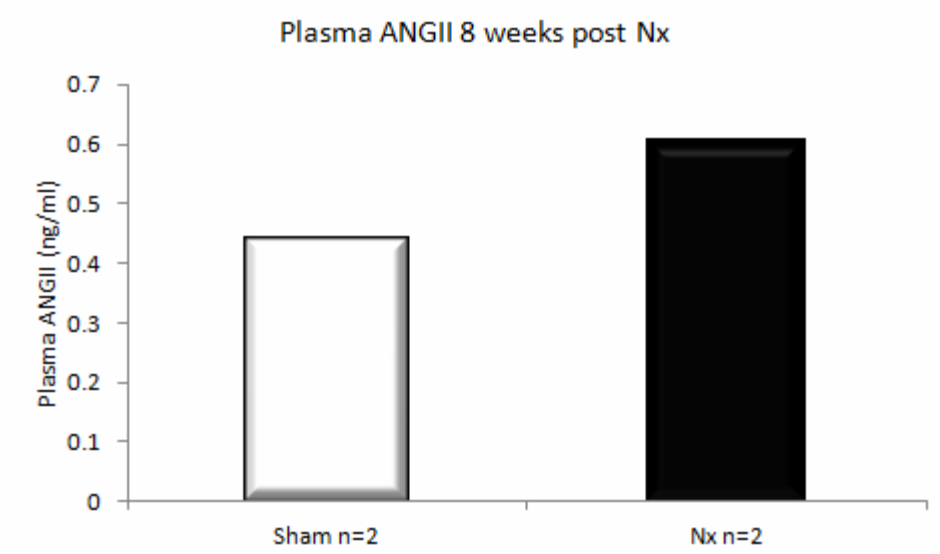

Figure 14: Plasma ANGII levels 8 weeks post-surgery. While an increase is observed in Nx animals, n values are not significant to make statistical conclusions.

Table 4: [^{13}N]Ammonia and [^{11}C]methyl-candesartan µPET results of Sham and nephrectomized animals 8 weeks post-surgery

	Sham	Nx
N	6	6
MBF	2.8±1.0ml/g/min	4.4±0.9ml/g/min*
RBF	6.7±2.4ml/g/min	6.4±2.4ml/g/min
Left Kidney DV	1.0±0.3ml/g	1.0±0.2ml/g

*$p<0.05$ compared to sham

5.1.5 [^{11}C]Methyl-Candesartan Characterization

Specific activity of [^{11}C]methyl-candesartan was recorded from 255.2-9925.3mCi/mmol and injected doses were 6.25E-4 to 2.99E-3µg/g, despite this large range, injected dose did not affect DV values (Fig 15). Both control and nephrectomized groups [^{11}C]methyl-candesartan scans had similar time activity curves (Fig 16). Test re-test variability between two users using partial volume loss corrected DVs was found to be 15% ±10% and a high intraclass correlation coefficient (0.91) (Fig 17).

5.1.6. [^{11}C]Methyl-Candesartan µPET

The plasma input correction factor (1.58) which was applied to DV values of the left kidney. DV values were found to be similar between sham and nephrectomized animals (Table 4).

Upon application of the 40-80 partial volume correction method to account for varying cortical thicknesses, a 40% decrease was observed in left kidney µPET measurements ($p<0.05$) (Fig 18). [^{11}C]Methyl-candesartan uptake was not observed in cardiac tissue.

5.1.7. Biodistribution

%ID/g displayed similar results in left kidney cortex and outer medulla as compared to µPET findings. Nephrectomized animals exhibited a 40% lower %ID/g (normalized to rat weight) than sham animals. Left kidney outer medulla in nephrectomized animals displayed a reduction of 55% %ID/g compared to sham rats (Fig 19).

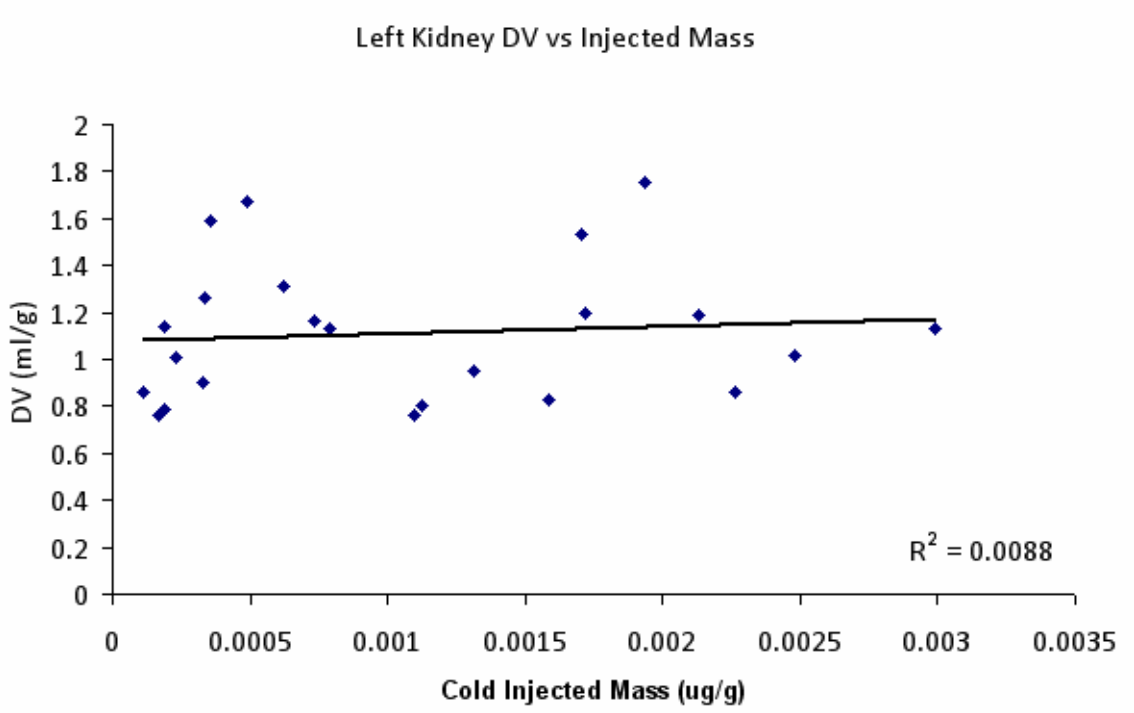

Figure 15: Left kidney (LK) Distribution Volumes (DV) (ml/g) vs Standardized Cold Injected Mass (µg/g) of individual scans. (Nx animal model)

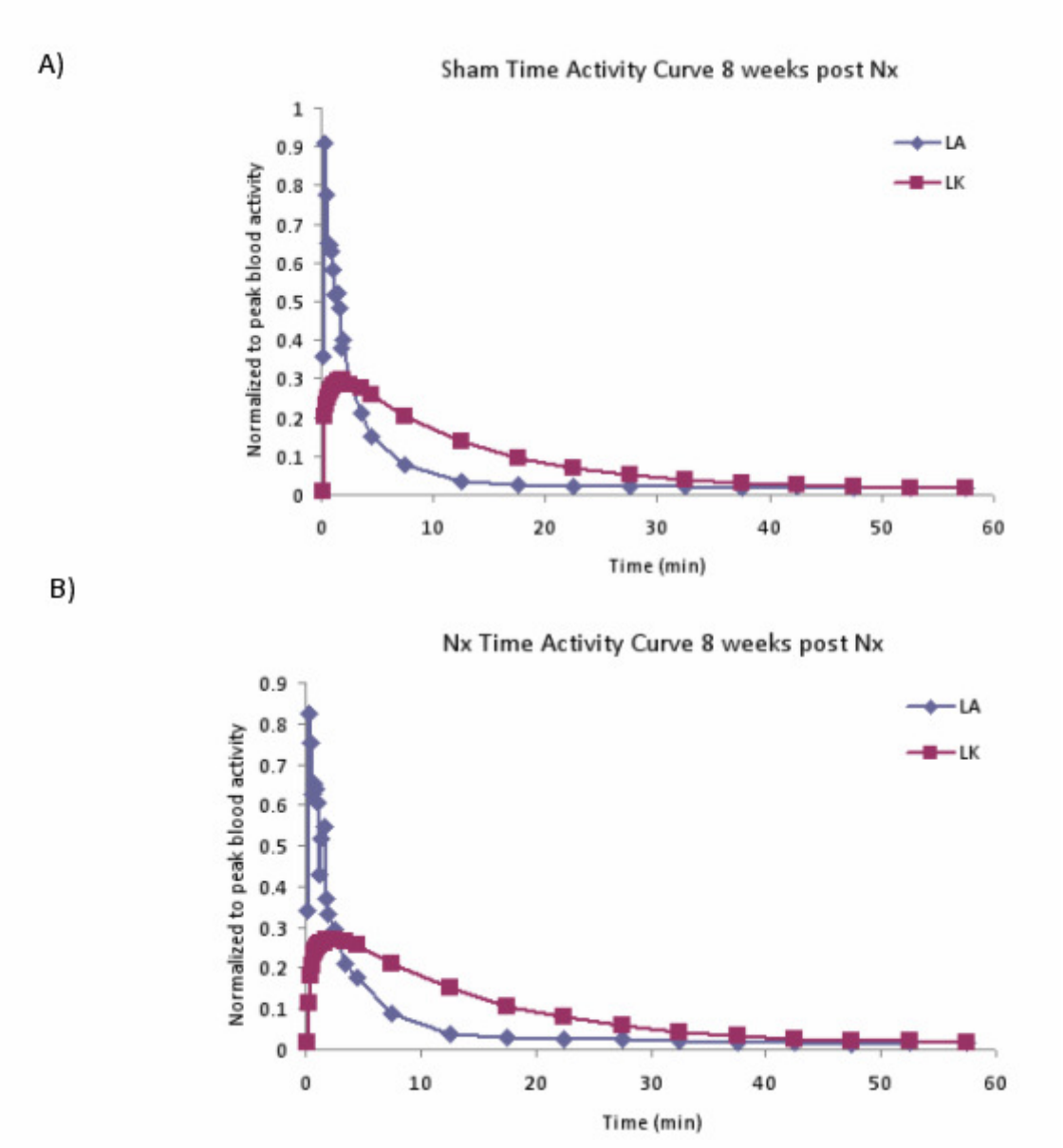

Figure 16: Time activity curve of [^{11}C]methyl-candesartan scan of sham (A) and Nx (B) animals 8 weeks post-surgery. Blood input (Left Atrium, LA) and Left Kidney (LK). Activity values are normalized to peak blood value and averaged.

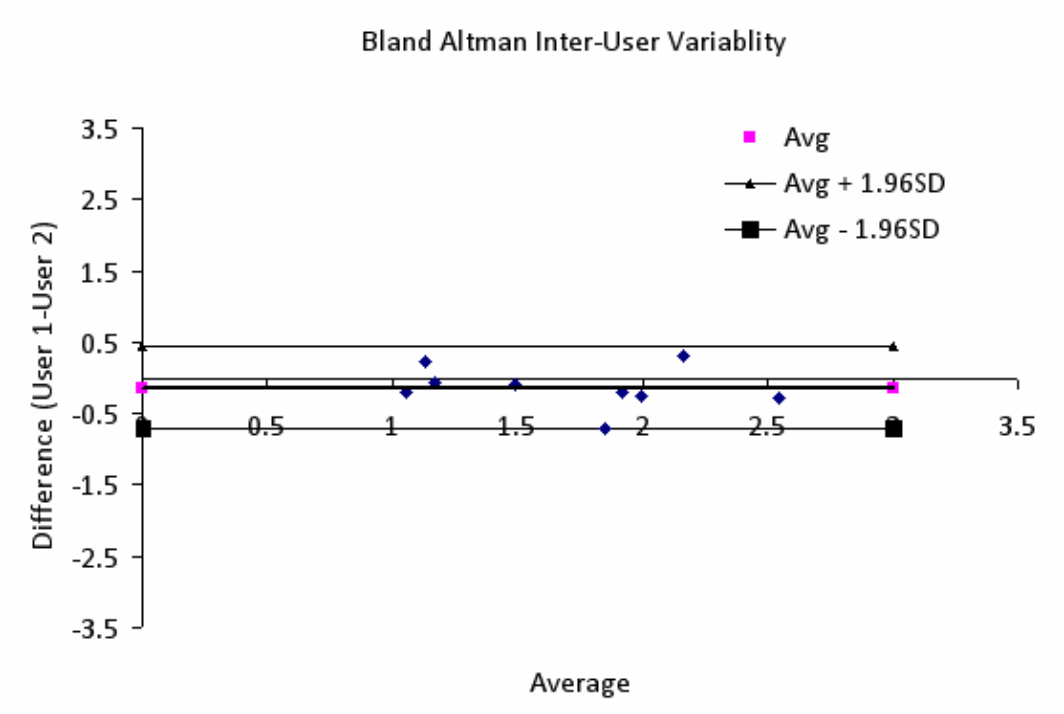

Figure 17: Bland Altman plot representing inter-use (2 observers) variability in partial volume corrected DV values. (15% ±10% inter user variability).

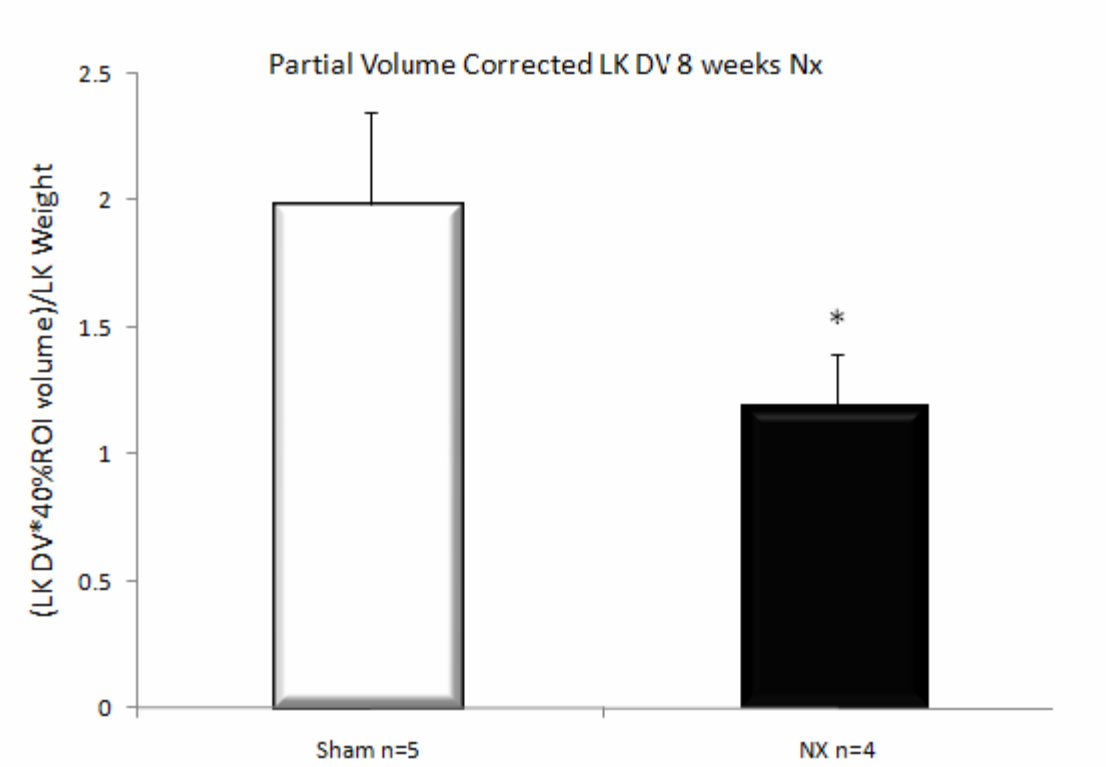

Figure 18: [^{11}C]Methyl-candesartan left kidney distribution values after partial volume loss correction using 40-80 method. *p<0.05

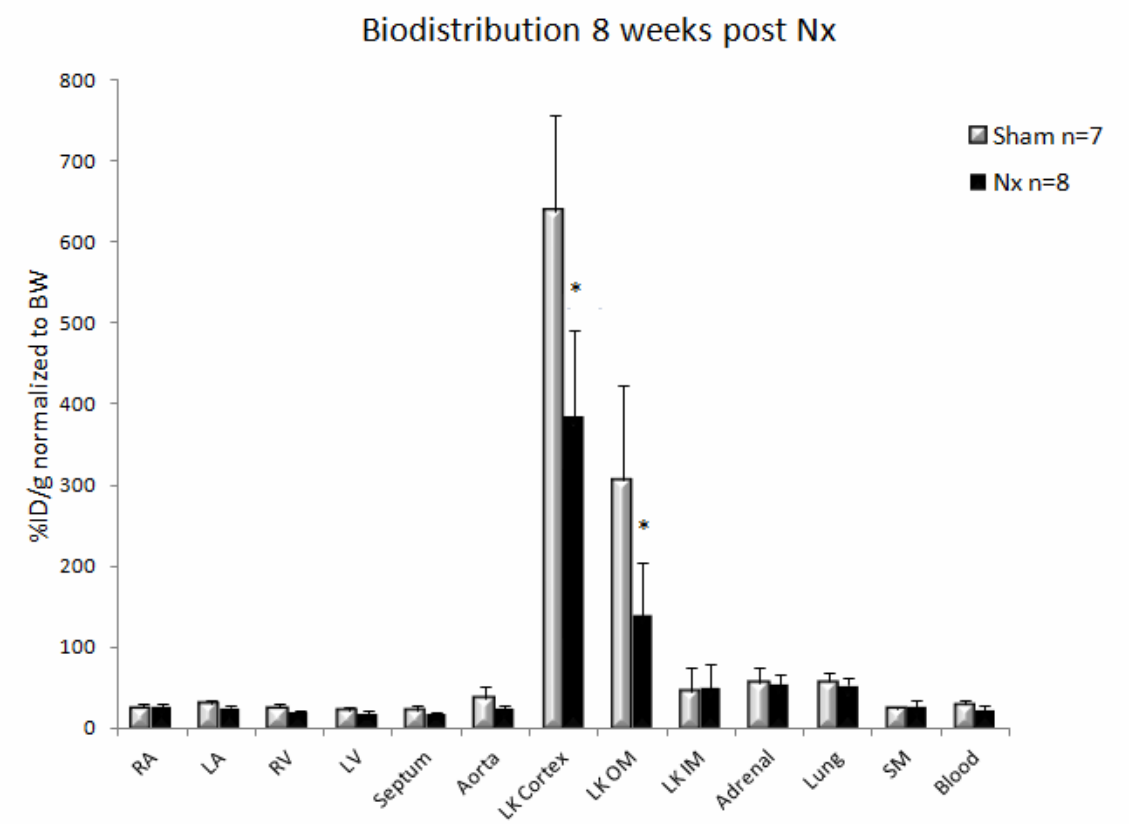

Figure 19: Biodistribution results 15min following [^{11}C]methyl-candesartan injection. *p<0.05

5.1.8. Western Blot

Analysis of kidney cortex showed a 24% decrease in nephrectomized animals when compared to aged matched controls ($p<0.05$). While the decrease is not as extensive as that measured by 40-80 µPET method, the trend is consistent with *in vivo* µPET findings (Fig 20). No change in LV AT_1R was measured using Western blot analysis (Fig 21). All bands were normalized to GAPDH loading control. The bands used for analysis was the unglycosylated form of the receptor.

5.2. Ligation-Reperfusion Model

5.2.1. Body and Organ Weights

At the end of the study, no change in body, heart and kidney weights between all groups were measured compared to sham (Table 5).

5.2.2. Echocardiography

Echocardiography was used to measure EF and FS to determine heart function. These values were similar in all transient ligation groups compared to control at 2 weeks post-surgery (Table 5). A 15% decrease in EF and 20% FS were found in permanent ligation animals (Table 5) ($p<0.05$).

5.2.3. Plasma ANGII

Plasma ANGII measurements were not successfully attained using the EIA kit mentioned in the methodology section. There was high level of variability within groups and between attempts that made the results unreliable (Fig 22).

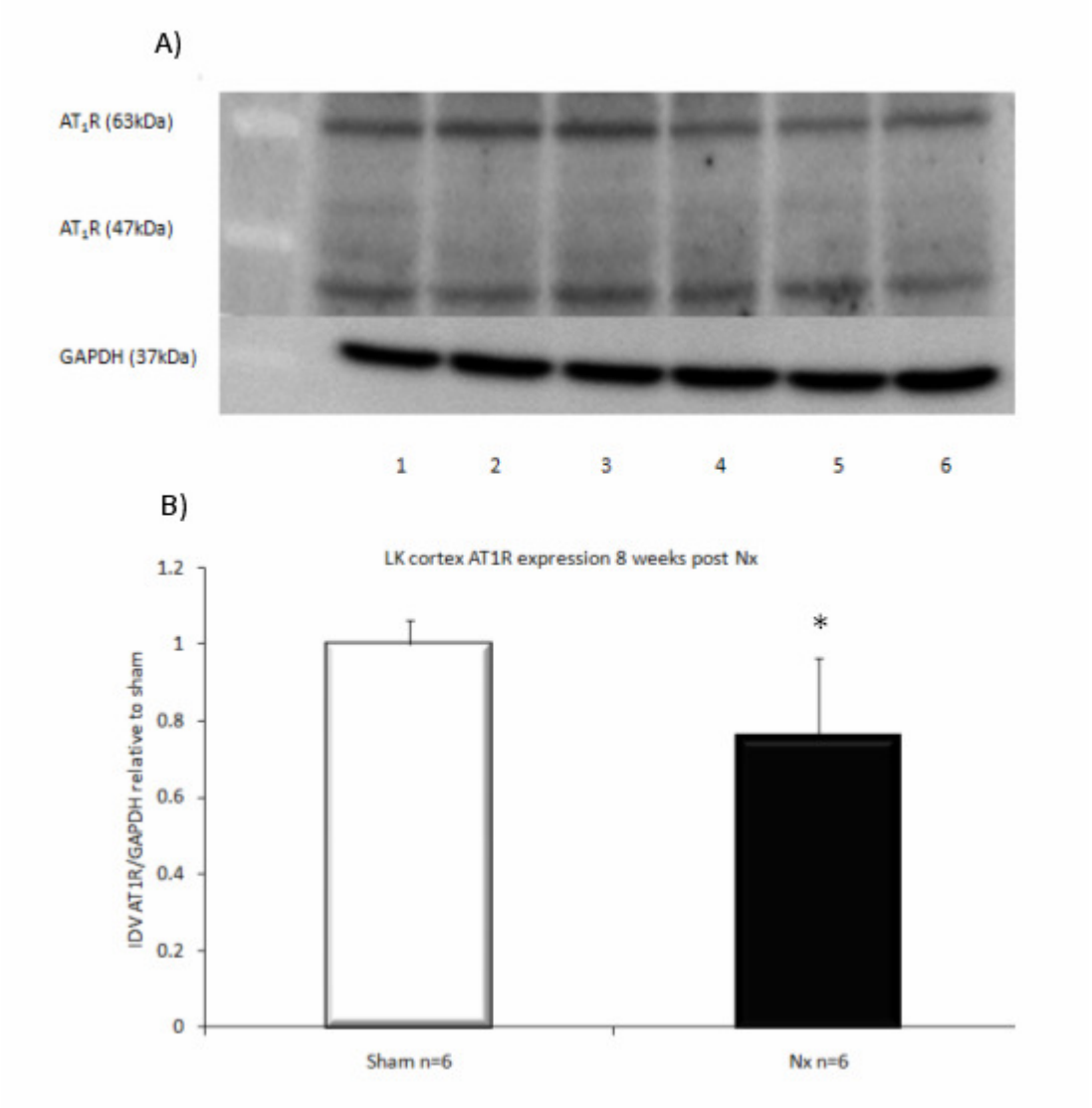

Figure 20: A) Representative left kidney Western blot Lane 1-3 Sham, Lane 4-6 nephrectomy B) Average AT_1R integrated density value (IDV) of sham and nephrectomized left kidney. *$p<0.05$

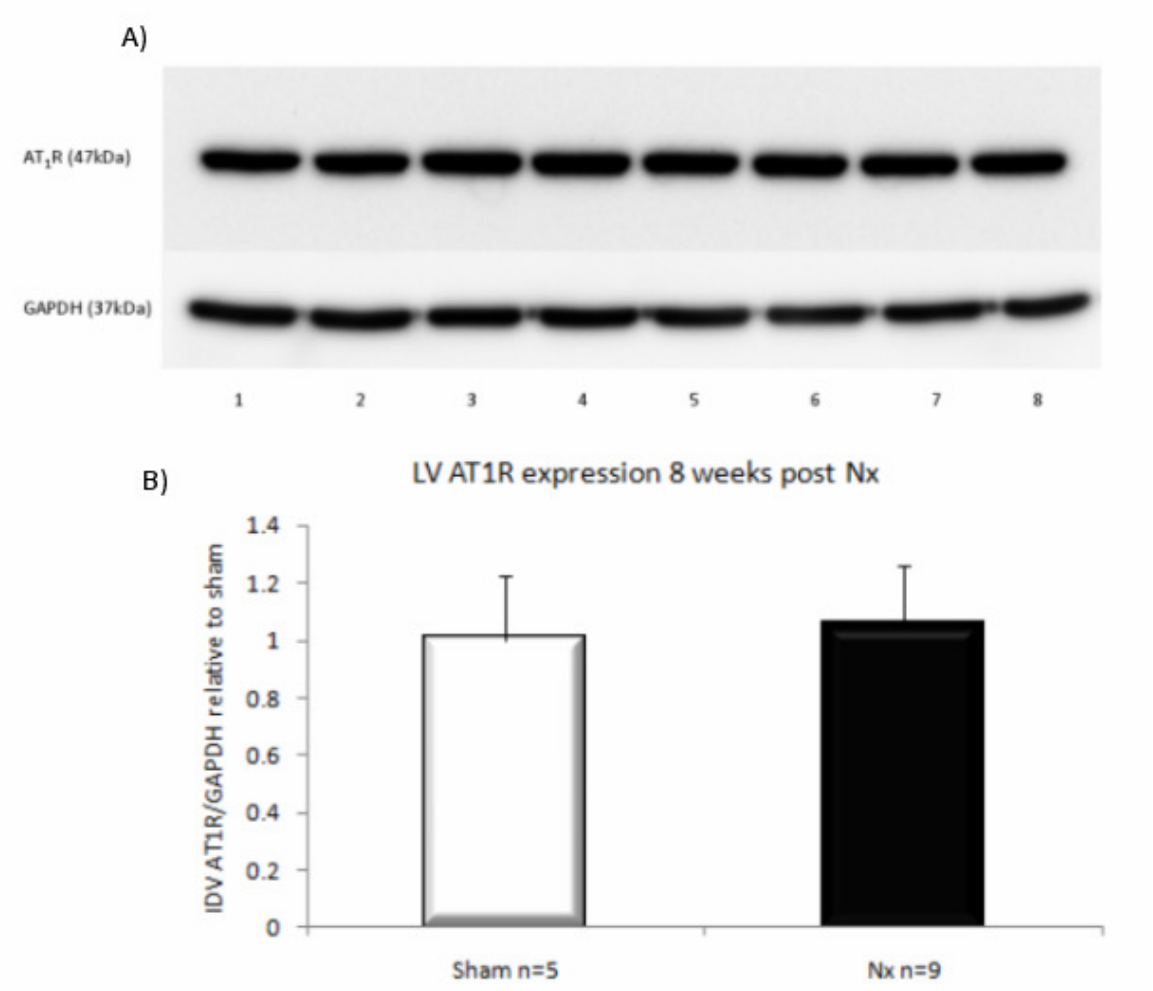

Figure 21: A) Representative Western blot Lane 1-4 Sham, Lane 5-8 Nx B) LV AT_1R between Nx animals and aged matched controls 8 weeks post-surgery

Table 5: Body Weight, Heart Weight, Kidney Weight, Ejection Fraction and Fractional Shortening in Sham, 3min, 5min, 20min and permanent (MI) ligation animals 2 weeks post-surgery

	Sham	3min	5min	20min	MI
n	5	5	5	5	5
BW	382±34.8g	362±4.5g	362±11.5g	392±48.7g	383±53.2g
HW/BW	0.0032±0.04	0.0034±0.04	0.0033±0.01	0.0035±0.03	0.0037±0.04
LKW/BW	0.0035±0.04	0.0036±0.02	0.0042±0.09	0.0035±0.03	0.0035±0.03
RKW/BW	0.0035±0.04	0.0036±0.02	0.0037±0.05	0.0033±0.03	0.0035±0.02
EF	75.3±7.2%	81.5±3.9%	70.3±13.4%	72.6±11.4%	53.4±8.9%*
FS	58.6±7.1%	64.4±3.6%	52.8±10.4%	56.0±8.0%	36.8±6.3%*

*p<0.05 compared to sham

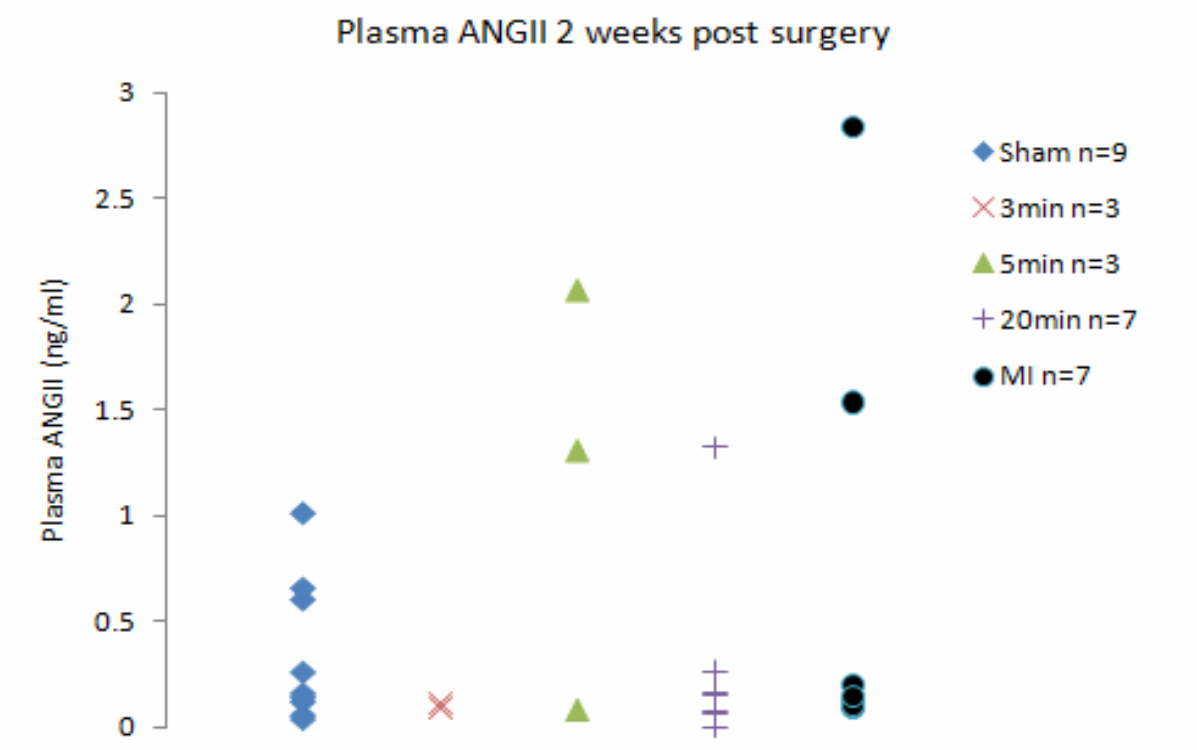

Figure 22: Plasma ANGII results from EIA kit using sham, 3min, 5min, 20min and permanent ligation animals. As seen here, results are inconsistent and no conclusions can be made.

5.2.4. [^{13}N]Ammonia µPET

For transient ligation groups (3, 5, or 20min), ratio of MBF in LAD region to contralateral region was comparable to sham operated animals. However, a 65% decrease in this ratio was observed in permanent ligation animals compared to sham (Table 6) (Fig 23).

5.2.5. [^{11}C]Methyl-Candesartan Characterization

Specific activity of [^{11}C]methyl-candesartan ranged from 73-5827 mCi/mmol and injected doses from 6.25E-4 to 1.08E-2µg/g. Cold mass injected doses did not affect DV values measured (Fig 24). [^{11}C]Methyl-candesartan scans displayed similar time activity curves in sham, 20min and permanent LAD ligation groups (Fig 25).

5.2.6. [^{11}C]Methyl-Candesartan µPET

The initial aim of this project was to measure *in vivo* changes in LV AT_1R levels in transient ligation animals using µPET, however no [^{11}C]methyl-candesartan uptake was observed in the heart (Fig 26).

Left kidney was used to compare [^{11}C]methyl-candesartan DV values as the right kidney was obstructed by high spillover from the liver (Fig 26). DVs in 3min, 5min, 20min and permanent ligation kidneys were all similar to sham values (Fig 27).

5.2.7. Western Blot

Western blot results from kidney cortex found no changes between transient and permanent ligation groups and sham animals. These results are consistent with the DV values obtained from µPET analysis (Fig 28).

Table 6: Ratio of MBF in LAD supplied LV flow/remote LV flow. Significant decrease is found in the permanent ligation (MI) is found 2 weeks post-LAD ligation surgery

Group	*n*	*Flow in LAD supplied LV (ml/g/min)*	*Flow in remote LV (ml/g/min)*	*Ratio (LAD/Remote)*
Control	9	3.2±0.8	3.8±1.2	0.85±0.1
3min	5	3.1±0.5	3.2±0.7	0.84±0.1
5min	3	2.6±0.2	3.2±0.3	0.79±0.02
20min	6	2.4±0.7	3.3±0.3	0.75±0.2
MI	7	0.9±0.4†	3.0±0.8	0.30±0.1†

†$p<0.001$ compared to baseline

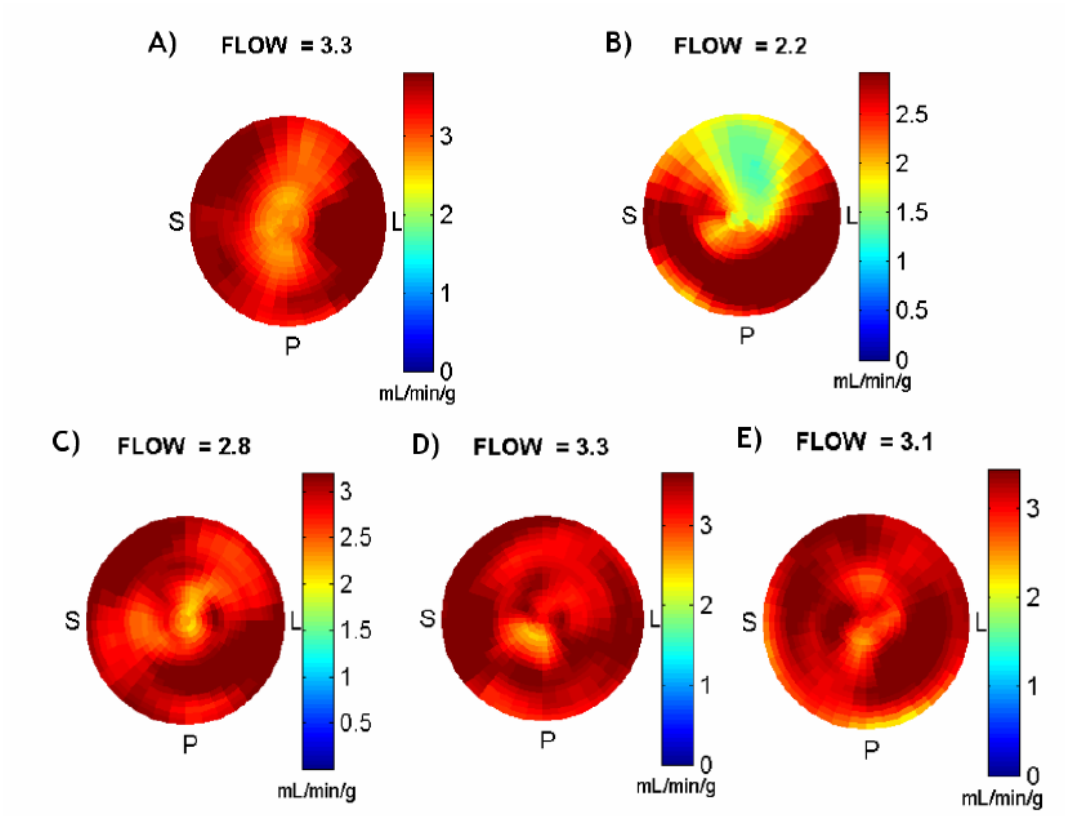

Figure 23: [^{13}N]NH_3 PET scan representative polar maps of A) Baseline B) Permanent Occlusion C) 3min ligation D) 5min ligation and E) 20min ligation. Obvious defect is visible only in permanent occlusion polar map (represented by green pixels).

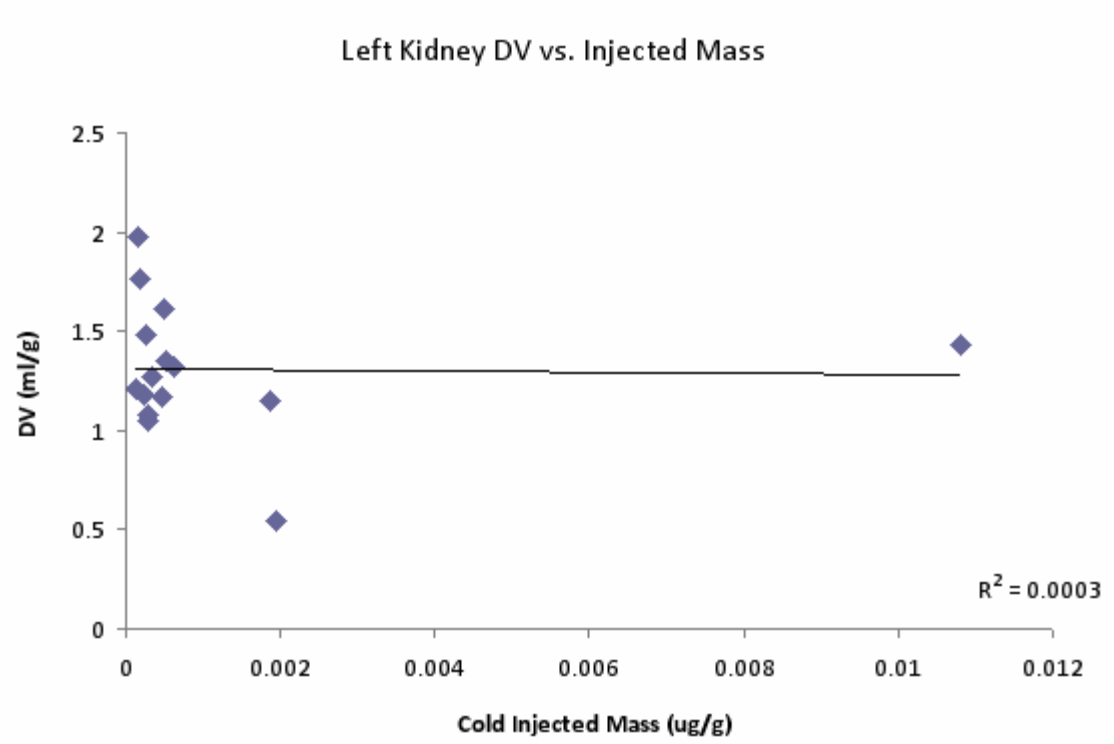

Figure 24: Left kidney Distribution Volumes (DV) (ml/g) vs Standardized Cold Injected Mass (µg/g) of individual scans. (LAD Ligation/Reperfusion animal model)

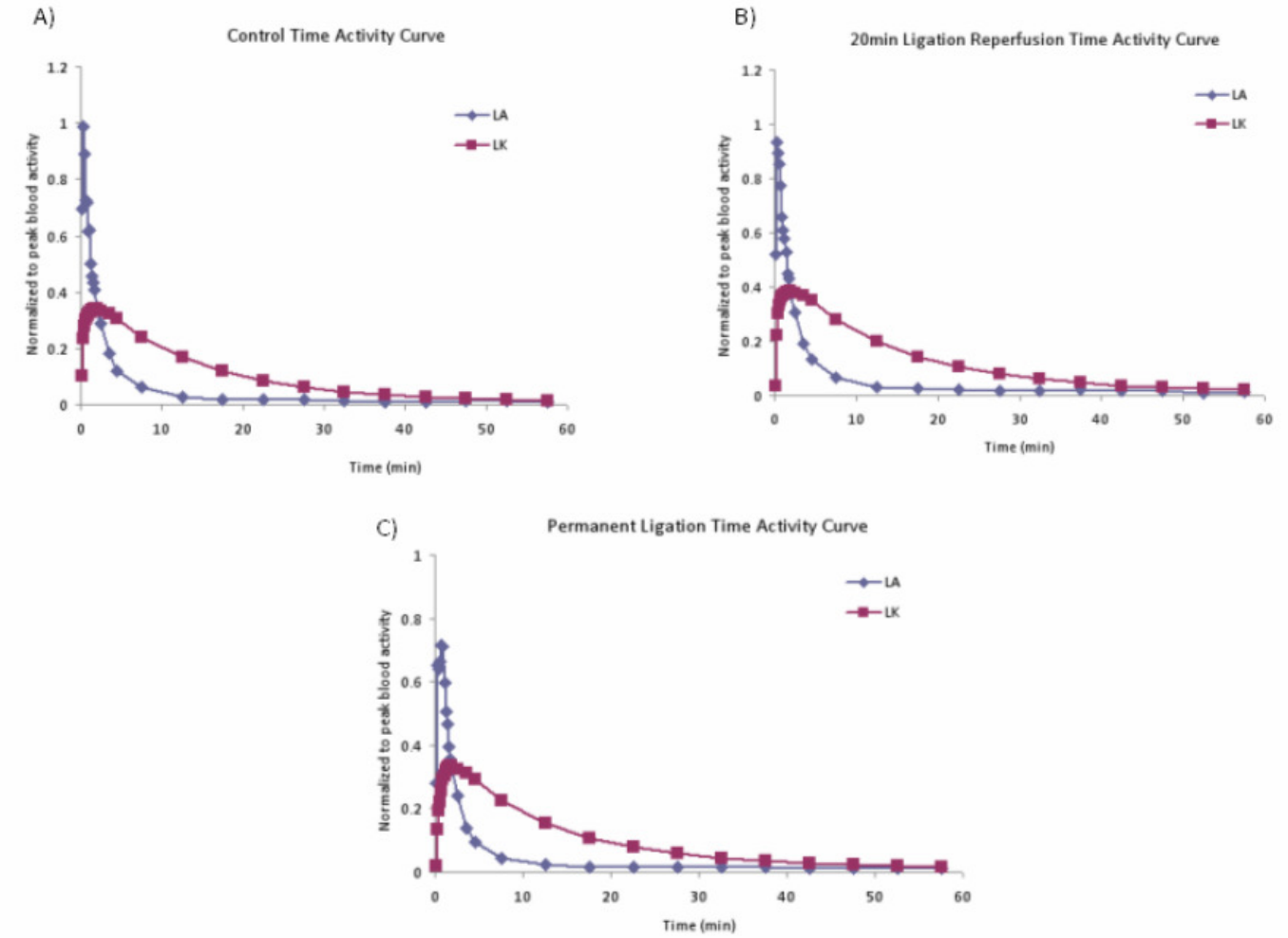

Figure 25: Time activity curve of [^{11}C]methyl-candesartan scan of control (A), 20min (B) and MI (C) animals. Blood input (Left Atrium, LA) and Left Kidney (LK). Activity values are normalized to peak blood value and averaged.

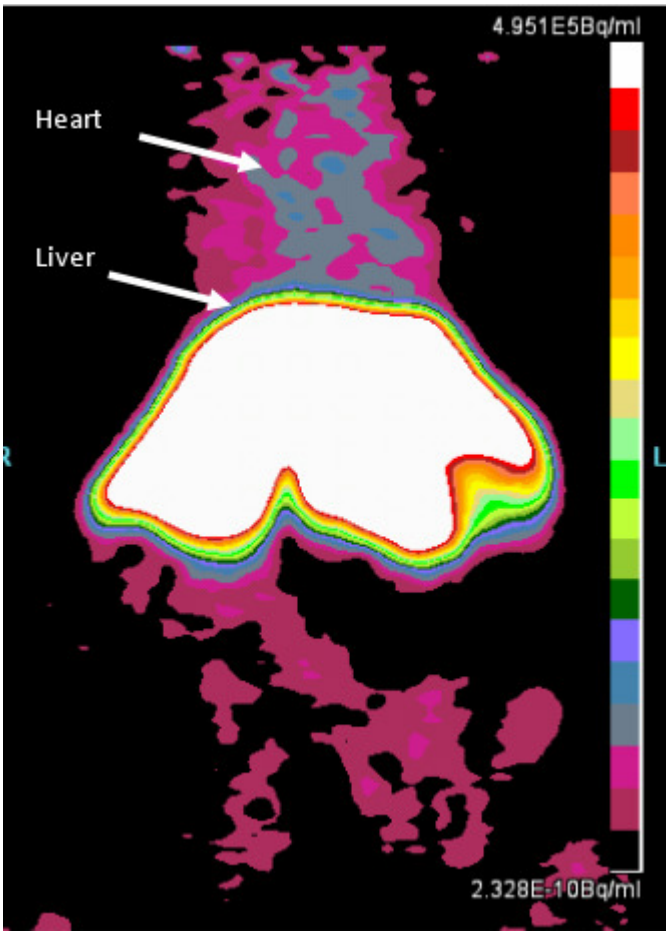

Figure 26: Representative image of [^{11}C]methyl-candesartan PET scan. Liver shows high uptake while heart uptake is at background levels.

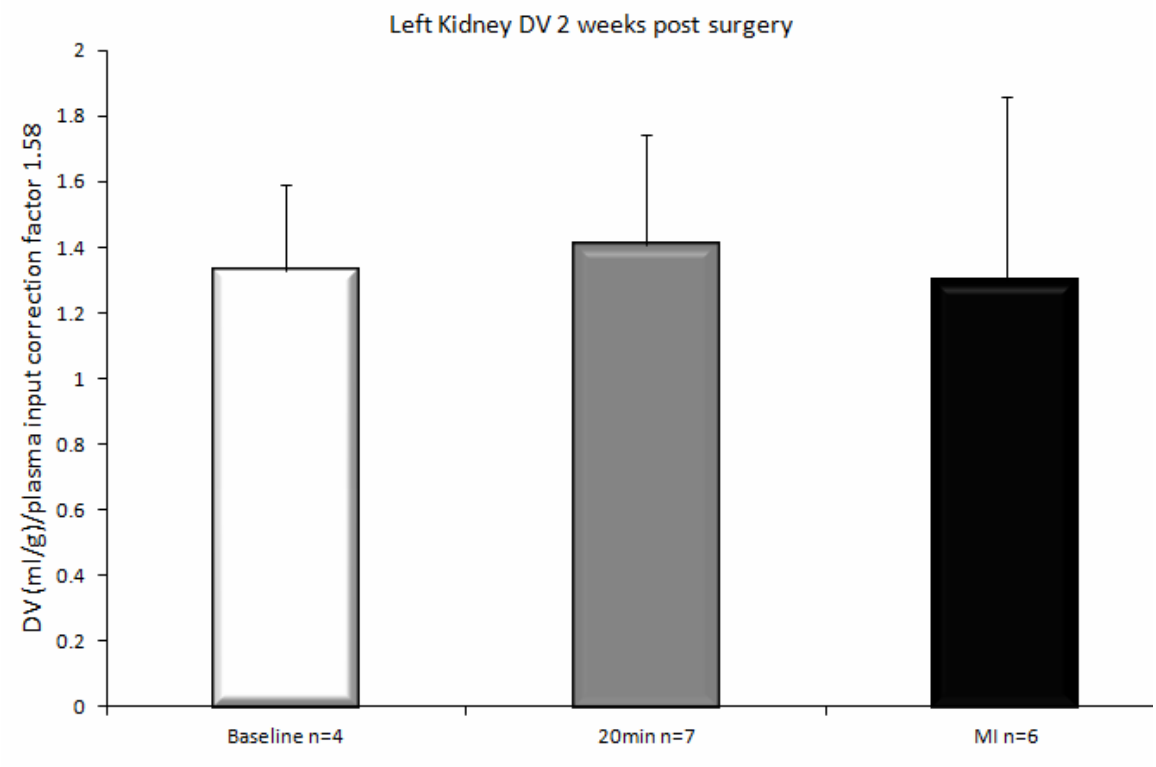

Figure 27: [^{11}C]Methyl-candesartan scan results. Left Kidney (LK) DV values show no change between control, 20min and permanent (MI) ligation group.

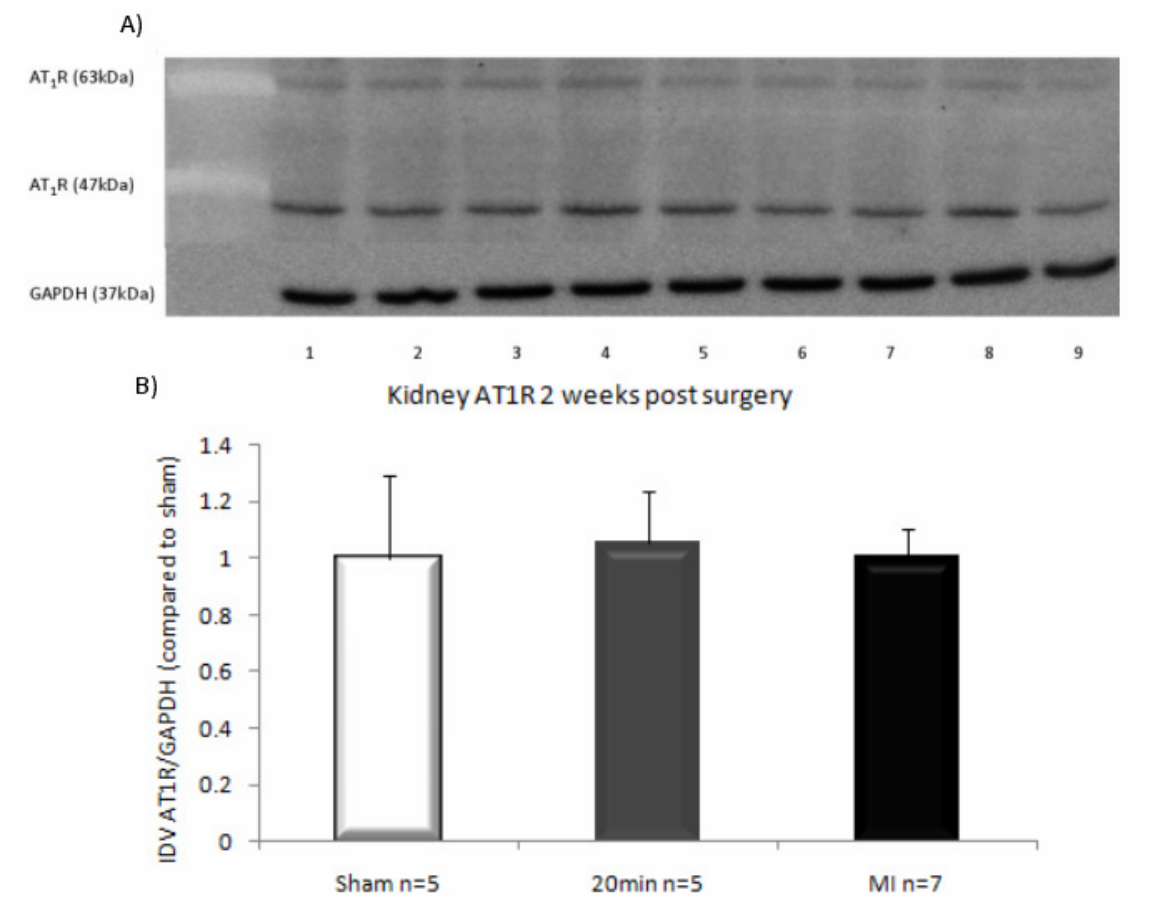

Figure 28: A) Representative Western Blot Lane 1-3 Sham, 4-6 MI, 7-9 20min ligation B) No change in renal cortex AT_1R between sham controls, 20min and permanent (MI) ligation group.

Areas that were deemed at risk were isolated from LV tissues upon sacrifice. Area at risk is used to describe LV area that is normally supplied by the LAD. Western blot analysis of the areas at risk for sham, 3min, 5min, 20min and permanent ligation groups, found that a significant increase in AT_1R expression was measured in the 20min (60%) and permanent ligation (115%) animals (Fig 29).

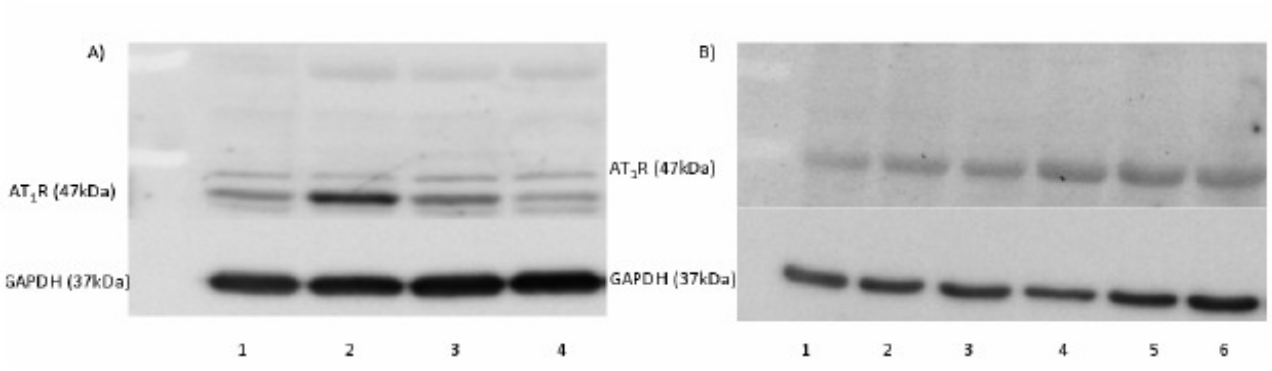

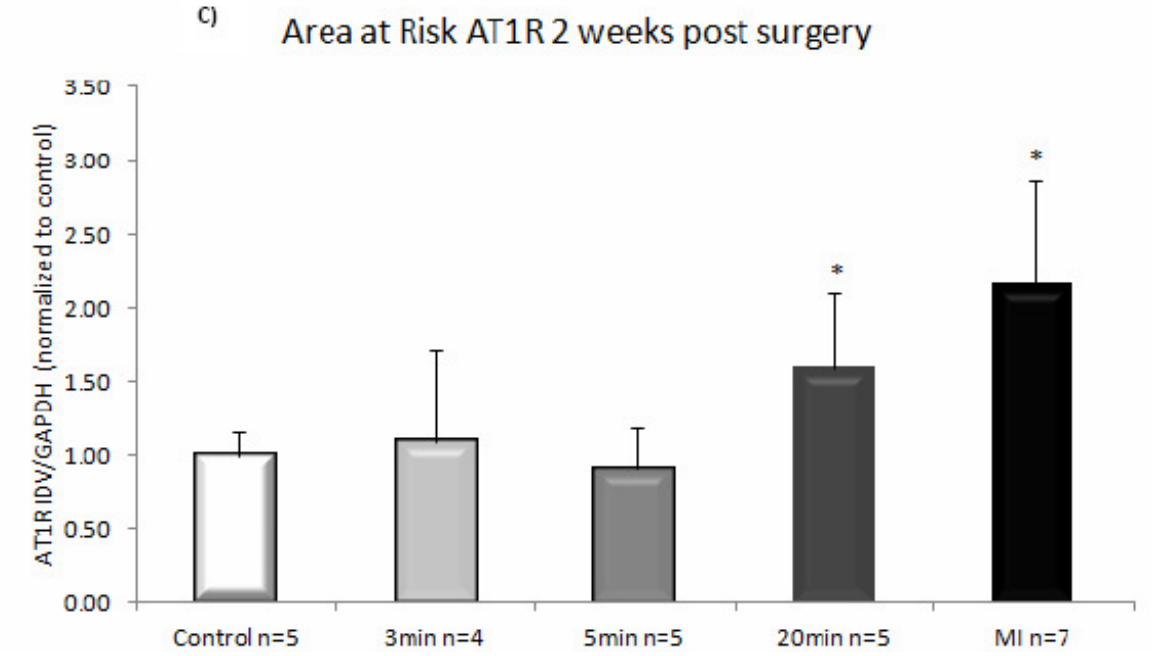

Figure 29: Representative Western blot of Area at risk A) Lane 1 Sham, Lane 2 MI, Lane 3 3min ligation, Lane 4 5min ligation B) Lane 1-3 Sham, Lane 4-6 20min ligation. C) MBF (white bars) shows significant decrease in MI group while transient ligation (3, 5 and 20min) have preserved MBF. AT_1R expression, as measured by Western Blot, shows significant increase in 20min and permanent (MI) ligation group. *$p<0.05$ vs control, †$p<0.001$ vs control

6. Discussion

6.1. 5/6 Nephrectomy Model

6.1.1. Body and Organ Weights

Heart weight to body weight ratio showed an increase of approximately 20% in nephrectomized animals which is consistent with other studies measuring heart weights at similar time points (Elkareh et al. 2007; Kennedy et al. 2008; Sviglerova et al. 2010). Remnant left kidney weights have been documented to be approximately 30% larger compared to intact left kidneys of sham animals 8 weeks post-surgery (Joly et al. 2005; Piecha et al. 2008). The increase kidney size is an effect known as compensatory kidney hypertrophy (Santos et al. 2006). Reduction of nephron numbers leads to chronic hyperfiltration which is followed by glomerular hypertrophy. The increase in kidney size is associated with increased cell size rather than increased cell proliferation and increased protein content in cells due to a decrease in protein degradation (Johnson et al. 1966; Coe et al. 1967). Body weights between nephrectomized and sham animals have been reported to be similar (Sui et al. 2010). The increase in both kidney and heart weight suggests hypertrophy of these two organs.

6.1.2. Echocardiography

Diminished EF and FS is associated with the end-stage renal failure (Foley et al. 2000). Long term studies have shown a decrease in these parameters 6 months post-renal ablation surgery compared to sham (Toblli et al. 2008). The same report also claim that initially after nephrectomy, there is no change in EF or FS, therefore the 8 week time point may fall under this initial phase which would explain the lack of change

presented here. Preserved EF is observed clinically in early kidney disease (Edwards et al. 2008). While cardiac hypertrophy is evident by the heart weights presented here, the preserved EF and FS may suggest that 8weeks post-nephrectomy is insufficient time to produce LV dysfunction.

6.1.3. Plasma ANGII

The EIA kit to measure ANGII requires plasma to be treated with aprotinin, a trypsin inhibitor, which was not immediately added to blood samples. This caused results to be highly variable between trials and within trial groups. However, it was found that if aprotinin is added immediately at time of blood collection, plasma ANGII concentrations were more consistent within each group, however due to insufficient number of samples, no conclusions could be made (n=2 Nx, n=2 Sham). The results presented here suggest a trend toward increased circulating ANGII levels however, published literature describes an initial increase in circulating ANGII after 2 weeks post-surgery, followed by a decrease to sham levels at 7 weeks (Mackie et al. 2001). Our group continues to investigate the role of plasma ANGII in the progression of disease and we are optimizing this methodology for future studies.

ANGII distribution in the kidney can be described in both endocrine and paracrine ANGII. Endocrine ANGII implies circulating ANGII while paracrine describes intrarenally produced ANGII. The highest concentration of ANGII in the kidney is in the glomerulus and peritubular cell surfaces (Schalekamp et al. 2006). Schalekamp et al observed that the ANGII in the glomerulus is circulating ANGII while peritubular cells express locally synthesized ANGII indicating ANGII effects in the glomerulus are

endocrine and paracrine in the peritubular region. AT_1R are present on cells close to the ANGII positive cells. AT_1R are located on proximal convoluted tubules, where ANGII promotes sodium reabsorption (Llorens-Cortes et al. 1994; Pallone 1994; Koike et al. 1995; Miyata et al. 1999). AT_1R are also highly expressed on glomerular mesengial cells which are specialized smooth muscles cells that regulate blood flow in the glomerulus which in turn controls the glomerular filtration rate (Fukai et al. 1999). Because ANGII in the glomerulus is described as circulating ANGII (Schalekamp et al. 2006), increased plasma peptide levels could cause an increase in GFR which is not sustained as CKD progresses. GFR may increase initially due to increased circulating ANGII (Mackie et al. 2001), however elevated plasma ANGII is not maintained through progression of disease which may describe the loss of compensatory kidney function.

6.1.4. MBF and RBF

Increased MBF has been reported in patients with chronic kidney disease, for which subtotal nephrectomy is a model (Koivuviita et al. 2009). MBF is affected mainly by local demand for oxygen. Because of the increased heart weight measured at 8 weeks post-nephrectomy, it is not surprising that MBF would increase presumably caused by the increased oxygen demand of the enlarged heart.

RBF was not statistically different in remnant kidney compared to whole left kidney of control animals. Increased RBF associated with compensatory remnant kidney hypertrophy after renal mass reduction is a transient process. Immediately after nephrectomy, RBF increases and then returns to normal levels 5 days post-surgery (Kaufman et al. 1975; Chevalier et al. 1985; Young et al. 1998). The return to normal

levels after an initial increase could be explained by increased renal ANGII caused by injury which acts as a vasoconstrictor and therefore diminishes blood flow (Vaziri et al. 2007). In the present study, RBF was measured 8 weeks post-surgery, and no increase was observed which is consistent with the literature.

6.1.5. 40-80 Partial Volume Loss Correction Method

Once the 40-80 method correction was applied to DV values of sham and nephrectomy animals, a decrease was observed in [^{11}C]methyl-candesartan distribution in nephrectomized kidneys. The decrease in AT_1R was measured by three different methods, µPET, Western blot and biodistribution.

6.1.6. µPET Test-Retest Variability

DV values corrected using 40-80 method were found to be a reproducible measurement. Two users analyzed the nephrectomized and sham µPET [^{11}C]methyl-candesartan images independently. The variability between the two users was found to be low and 40-80 corrected DVs using the method described here was deemed reproducible.

6.1.7. Renal AT_1R

An increase in renal AT_1R was expected 8 weeks after nephrectomy however, a decrease was measured instead. While these results were surprising as they disagree with the initial hypothesis, they do correspond to results obtained from 40-80 µPET analysis. There is a discrepancy between the degree of decrease found in µPET and Western blot analyses. This could be explained by the presence of intracellular AT_1R that may not be altered to the same degree as plasma membrane receptors. While

traditionally GPCRs are thought to exist primarily on the cell surface, there is increasing evidence that these receptors, including AT_1R, exist within the cell (Gobeil et al. 2006; Goetzl 2007; Boivin et al. 2008; Pendergrass et al. 2009). The study of intracellular AT_1R expression in response to renal injury is not well documented however if the regulation of intracellular and surface AT_1R differ in response to disease, the Western blot analysis will be skewed and may not match *in vivo* μPET analysis, as [^{11}C]methyl-candesartan is expected to bind only to surface receptors. If the intracellular AT_1R are regulated differently or are decreased to a lesser extent than the surface receptors, the whole cell lysates will show an underestimated decrease in AT_1R, which could have been the case in the results presented here.

The decrease in [^{11}C]methyl-candesartan DV measured with μPET was very intriguing as it was consistent with *in vitro* findings. Joly et al examined AT_1R mRNA and expression changes in mice 4 weeks post-subtotal nephrectomy and found a 33% decrease in AT_1R mRNA and diminished immunostaining of AT_1R in the renal cortex (Joly et al. 2005). The receptor is mostly found in proximal convoluted tubules (PCT) in the cortex, the brush borders of these cells are destroyed in remnant kidneys following renal ablation. It was suggested that this decrease in AT_1R mRNA and cell surface protein levels was a physiological response to increase intrarenal ANGII. AT_1R could be downregulated to avoid the deleterious effects of ANGII in renal disease. The decrease in mRNA is corroborated with decreased binding density of AT_1R in remnant kidney in another study examining AT_1R reduction 4 weeks post-renal ablation (Cao et al. 2002). AT_1R has a higher density PCT when compared to other nephron segments (Harrison-

Bernard et al. 1997). PCT cells are responsible for sodium and bicarbonate reabsorption from the tubular lumen into the peritubular capillaries. A Na^+/H^+ exchanger on the apical surface brings Na^+ into the cell while Na^+-HCO_3^- (bicarbonate) cotransporter and Na^+/K^+ ATPase on the basolateral membrane work to transfer HCO_3^- to the blood stream and keep intracellular Na^+ levels low to promote a concentration gradient compared to the lumen (Kobori et al. 2009). AT_1R are present on both apical and basolateral membranes of PCT cells. 5/6 Nephrectomy leads to an increase in bicarbonate reabsorption rate which is inhibited by losartan treatment (Levine et al. 1997). On the apical side, ANGII through AT_1R activates Sodium Hydrogen Exchanger (NHE3) which causes Na^+ reabsorption in the proximal tubules (Banday et al. 2011).

Documented decrease in AT_1R in renal injury could be associated with AT_1R's role adipogenesis inhibition. In a study looking at nephrectomized rats 10 months post-surgery, a decrease in renal AT_1R protein expression and an increase in AT_2R were found. This change was thought to have been due to the ectopic fat deposition observed in renal ablation surgery models. Ten months after surgery, sham animals evinced fat deposition limited to the renal sinus, however, in 5/6 nephrectomized animals adipocyte infiltration was observed in the cortex as well as the sinus (Sui et al. 2010). These fat deposits were surrounded by macrophage derived foam cells (Sui et al. 2010). Excess fat in visceral organs is a common effect in diseases such as cardiovascular disease and chronic renal disease. AT_2R is associated with adipocyte differentiation while AT_1R is thought to inhibit adipogenesis (Jones et al. 1997). Both effects are thought to be mediated through peroxisome proliferator activated receptor γ (PPARγ), an important receptor involved in

adipocyte maturation which is upregulated in the unilateral nephrectomy model (Rosen et al. 2000; Janke et al. 2006). Therefore, the increase in fat accumulation may be because of the activation of AT_2R and the down regulation of AT_1R. The increase in AT_2R and PPARγ and decrease in AT_1R is attenuated by treatment with ACEi, thereby diminishing fat deposits in the remnant kidney. A decrease in kidney ANGII by ACEi treatment would attenuate the downregulation of AT_1R by consistent exposure to ANGII.

It cannot be ignored that there is evidence suggesting the opposite effect in AT_1R expression following renal ablation which was the basis of the initial hypothesis of this project. Increases in AT_1R protein expression measured by Western blot have been documented in other studies (Vaziri et al. 2007; Zhao et al. 2010). While it is not agreed upon how the intrarenal RAS reacts to renal failure, it is consistent that the RAS is somehow dysregulated.

The role of AT_2R in the progression of renal disease is also suggested by Cao and colleagues (Cao et al. 2002). This group reported the benefits of blocking AT_2R in an animal model of renal ablation. AT_2R blockade decreased proteinuria, osteopontin (chemokine) expression, accumulation of macrophages and proliferation in remnant kidney(Cao et al. 2002). AT_2R antagonism also attenuated nephrin deficiency, which is observed in experimental and human nephropathies (Kestila et al. 1998; Topham et al. 1999; Kawachi et al. 2000; Benigni et al. 2001; Bonnet et al. 2001). Nephrin is a transmembrane protein of the Ig superfamily that localizes in the slit pore of podocytes in the glomerulus and plays an important role in maintaining the integrity of the

filtration barrier (Tanaka et al. 1999; Kawachi et al. 2000; Benigni et al. 2001). This study suggests that the role of AT_2R may in fact be detrimental in renal disease.

The mechanistic pathway of renal diseases remains to be completely understood. The investigation of this pathway is a common theme in nephropathy studies. RAS is believed to play a role in progression of this disease as RAS blockade ameliorates proteinuria independently of its blood pressure lowering effects (Suzuki et al. 2007). The changes in AT_1R may be transient and PET is a useful tool to examine these changes in longitudinal studies over a longer time line. The conflicting results found in literature studying renal disease reflect the complexity of the mechanisms involved in its progression.

6.1.8. LV AT_1R

LV hypertrophy is common in end-stage renal failure and is associated with increased cardiac events and death in renal failure patients (Levy et al. 1987; Harnett et al. 1988; Koren et al. 1991). ACE and AT_1R blockade treatment protects against cardiac remodelling in late stages of renal disease (i.e. minimizing LV hypertrophy) suggesting a role of RAS in LV hypertrophy associated with renal failure (Amann et al. 1998; Dickhout et al. 2011). Locally produced ANGII may play a role in cardiac dysfunction and hypertrophy associated with renal disease. It is possible that while ANGII increases, AT_1R is unchanged which would explain the hypertrophy without increased receptor expression. Investigating a reliable method to measure cardiac ANGII would add depth to the understanding of altered RAS mechanism's role in cardiac hypertrophy in this animal model.

LV hypertrophy is also related to other traditional and nontraditional risk factors associated with CKD. Traditional risk factors include: hypertension, dyslipidemia and diabetes and non-traditional risk factors include: hyperparathyroidism, endothelial dysfunction, and inflammation (Moriguchi et al. 2011). A recent study demonstrated that these nontraditional factors were highly correlated to LV hypertrophy in a rat model of CKD (Moriguchi et al. 2011). While the RAS is though to have a role in LV hypertrophy associated with CKD, other factors are clearly at play.

6.2. Ligation-Reperfusion Model

6.2.1. Body and Organ Weights

Body and organ weights showed no change in sham, 3min, 5min, 20min or permanent ligation groups. Although cardiac hypertrophy is associated with heart failure which can be induced by permanent LAD ligation, the results presented here suggest that 2 weeks is not sufficient time for the animals to develop hypertrophy.

6.2.2. Echocardiography

EF and FS as measured by echocardiography displayed no significant change in the transient ligation groups, however a decrease was observed in permanent ligation animals. Decreased EF is associated with heart failure; therefore the results presented here suggest that 2 weeks following permanent LAD ligation rats show LV dysfunction and early stages of heart failure which is consistent with the literature (Ahmet et al. 2009). The preserved LV function in transient ligation groups indicate that LAD ligation followed by reperfusion did not cause enough damage to diminish EF and FS.

6.2.3. Plasma ANGII

The issues with this method of measuring plasma ANGII have been discussed (see section 6.1.3.). However, with the ligation/reperfusion animals the results were even more scatted than nephrectomized plasma. ANGII is a very sensitive peptide and is expressed in low levels in rat plasma (approximately 0.02ng/ml) (Campbell et al. 1999). Due to the sensitive nature of this protein, perhaps more care should be taken to prevent degradation. For instance, another paper measuring plasma ANGII used cold syringes to extract blood and processed the plasma immediately rather than keep samples for up to a month as was done here (Baylis et al. 1997). From the results presented here, the plasma ANGII levels range from 10.14E-5 to 2.84 ng/ml, and in some cases, the levels were deemed too low to be detected using this kit.

6.2.4. MBF and LV AT_1R

LAD region MBF was statistically decreased in permanent ligation group but preserved in transient ligation groups. The diminished flow in the permanent ligation group suggested that this model would not be appropriate for [^{11}C]methyl-candesartan scanning, as tracer would not have access to the area of interest. A permanently blocked LAD artery would prevent [^{11}C]methyl-candesartan from accessing the infarcted tissue, which is where the increase in AT_1R expression is localized. The preserved MBF in transient ligation group meant that whichever group (3, 5 or 20min) showed a change in LV AT_1R would be used as a model for further PET studies.

LV AT_1R levels were significantly increased in the permanent ligation group, which is consistent with studies discussed earlier. While 3 and 5min transient ligation groups

showed similar cardiac AT_1R expression to sham operated animals, 20min transient ligation animals showed a significant increase. Therefore it was concluded that because 20min transient LAD ligation model produced a significant increase in LV AT_1R levels while maintaining MBF to the region of interest, that this model would be used for further μPET studies as tracer would have access to the region of the LV of interest.

While the *in vitro* results showed the expected results, no uptake was seen in cardiac tissue using [^{11}C]methyl-candesartan μPET. This could be explained by the relatively low specific activity of this tracer. Higuchi et al successfully imaged the LV AT_1R using the same animal model with [^{11}C]KR31173, however this tracer has been reported to have specific activities of 6979 mCi/μmol while the average of our studies was 1967.7 mCi/μmol using gas phase production system (Mathews et al. 2004; Zober et al. 2006; Higuchi et al. 2010). Cardiac AT_1R levels are very low and are therefore easily saturated (Chang et al. 1991). Low specific activity means that more unlabeled cold methyl-candesartan is present in the injected dose. This cold methyl-candesartan would bind to the receptors and saturate these receptors to a level higher than the maximum 5% as described by Jagoda et. al for accurate receptor density inference from PET analysis (Jagoda et al. 2004). In previous competition studies using control animals, ARB treatment was only able to diminish [^{11}C]methyl-candesartan uptake in heart tissue using a very high dose of losartan (30mg/kg) (Hadizad et al. 2009). The lack of decrease in tracer uptake with candesartan and smaller doses of losartan suggests that the control signal is due to non specific binding. With a higher specific activity, more [^{11}C]methyl-candesartan would be available to bind to free AT_1R. Therefore, while

[^{11}C]methyl-candesartan shows great promise as a renal AT_1R imaging agent because of its positive AT_1R binding properties, specific activity must be increased before it can be used in cardiac imaging (Hadizad et al. 2009).

6.2.5. Renal AT_1R

Kidney cortex AT_1R was assessed both *in vivo* and *ex vivo* by PET scan and Western blot respectively. Both methods showed no change in renal cortex AT_1R levels 2 weeks post-surgery. Kidney AT_1R in a permanent ligation model was studied by Tan et al, and they found modest decreases in AT_1R levels at 4 weeks post-surgery (Tan et al. 2004). Therefore, perhaps with an extended time course a decrease would be measured in these animals but 2 weeks does not seem to be sufficient time to cause receptor changes. The PVE correction method was not applied to the PET analysis of this animal model as the size of the kidneys remained the same in all groups and therefore partial volume losses caused by different thicknesses in cortex was not a concern.

7. Conclusion

7.1. 40-80 Partial Volume Correction

The 40-80 correction applied to left kidney [^{11}C]methyl-candesartan was found to be a reliable method of analysis with low variability between users**.**

7.2. Nephrectomy Animal Model

Subtotal nephrectomy induced an increase in MBF, preserved RBF, normal EF, and cardiac and renal hypertrophy. AT_1R changes were altered in kidney cortex as measured by [^{11}C]methyl-candesartan μPET analysis and Western blotting. No change was found in LV AT_1R protein expression which was only measured by Western blot as [^{11}C]methyl-candesartan uptake was not observed in the heart.

7.3. Ligation-Reperfusion Animal Model

LAD ligation, both transient and permanent, did not cause a change in EF or FS. MBF in 3, 5 and 20min LAD ligation was maintained to sham levels 2 weeks after surgery. As expected, permanent LAD ligation caused a significant decrease in MBF. Renal AT_1R *in vivo* and *in vitro* measurements were comparable to sham animals in transient and permanent ligation groups. While 3 and 5min LAD ligations were not sufficient time to produce a change in LV AT_1R, permanent and 20min ligation induced an increase in LV receptor expression as observed via Western assays. The combination of increased cardiac AT_1R in the infarcted area with the preserved MBF to the area where the AT_1R expression increase is localized suggests that 20min LAD ligation/reperfusion animal model is suitable for future cardiac PET studies

8. Future Studies

8.1. ANGII Levels

Plasma ANGII was not successfully measured in this project. We are currently investigating other methods to assess ANGII levels in both nephrectomy and LAD ligation animal models. Plasma levels will be spiked with a known amount of ANGII to increase peptide to measurable levels. It would also be of great value to measure tissue ANGII levels. Understanding either cardiac or renal ANGII level changes will shed light on locally produced ANGII's role in disease progression and AT_1R expression.

8.2. Nephrectomy Animal Model

Quantitative assessment of disease characterization will be done in further studies. Serum creatine levels, urinary protein levels, glomerulosclerosis, blood pressure using telemetry will be measured to further investigate response to RAS blockade

8.3.Ligation-Reperfusion Animal Model

The main focus of the continuation of this part of the project lies in the improvement of specific activity of tracer. Optimization of [^{11}C]methyl-candesartan synthesis is ongoing. Our group is also working on an F^{18} labelled Losartan compound which will ideally lead to higher specific activity, making cardiac AT_1R imaging possible. We also hope to translate [^{11}C]methyl-candesartan to human imaging.

9. References

Ahmet, I., E. Spangler, et al. (2009). "Survival and cardioprotective benefits of long-term blueberry enriched diet in dilated cardiomyopathy following myocardial infarction in rats." PLoS One **4**(11): e7975.

Aiyar, N., E. Baker, et al. (1994). "Human AT1 receptor is a single copy gene: characterization in a stable cell line." Mol Cell Biochem **131**(1): 75-86.

Akishita, M., M. Horiuchi, et al. (2000). "Inflammation influences vascular remodeling through AT2 receptor expression and signaling." Physiol Genomics **2**(1): 13-20.

Allen, A. M., J. Zhuo, et al. (1999). "Localization of angiotensin AT1 and AT2 receptors." J Am Soc Nephrol **10 Suppl 11**: S23-9.

Allen, A. M., J. Zhuo, et al. (2000). "Localization and function of angiotensin AT1 receptors." Am J Hypertens **13**(1 Pt 2): 31S-38S.

Amann, K., I. Rychlik, et al. (1998). "Left ventricular hypertrophy in renal failure." Kidney Int Suppl **68**: S78-85.

Antoun, R., T. Hadizad, et al. (2010). "In vivo evaluation of [^{11}C]methyl-Losartan as a selective AT_1R radioligands in rats." J Nucl Med **51**(Supplement 2): 1490.

Aoyagi, T., Y. Izumi, et al. (2008). "Vasopressin regulates the renin-angiotensin-aldosterone system via V1a receptors in macula densa cells." Am J Physiol Renal Physiol **295**(1): F100-7.

Banday, A. A. and M. F. Lokhandwala (2011). "Angiotensin II-mediated biphasic regulation of proximal tubular Na+/H+ exchanger 3 is impaired during oxidative stress." Am J Physiol Renal Physiol **301**(2): F364-70.

Barreras, A. and C. Gurk-Turner (2003). "Angiotensin II receptor blockers." Proc (Bayl Univ Med Cent) **16**(1): 123-6.

Baylis, C., K. Engels, et al. (1997). "Plasma renin activity and metabolic clearance rate of angiotensin II in the unstressed aging rat." Mech Ageing Dev **97**(2): 163-72.

Bayorh, M. A., A. A. Ganafa, et al. (2005). "Alterations in aldosterone and angiotensin II levels in salt-induced hypertension." Clin Exp Hypertens **27**(4): 355-67.

Benigni, A., S. Tomasoni, et al. (2001). "Blocking angiotensin II synthesis/activity preserves glomerular nephrin in rats with severe nephrosis." J Am Soc Nephrol **12**(5): 941-8.

Berk, B. C. (2003). "Angiotensin type 2 receptor (AT2R): a challenging twin." Sci STKE **2003**(181): PE16.

Bernstein, K. E. and M. B. Marrero (1996). "The Importance of Tyrosine Phosphorylation in Angiotensin II Signaling." Trends Cardiovasc Med **6**(6): 179-87.

Boivin, B., G. Vaniotis, et al. (2008). "G protein-coupled receptors in and on the cell nucleus: a new signaling paradigm?" J Recept Signal Transduct Res **28**(1-2): 15-28.

Bonnet, F., M. E. Cooper, et al. (2001). "Irbesartan normalises the deficiency in glomerular nephrin expression in a model of diabetes and hypertension." Diabetologia **44**(7): 874-7.

Bravo, P., K. Fukushima, et al. (2011). "Translational imaging of the myocardial angiotensin II type 1 receptor using C-11 KR31173 PET: From animal model to human application." J Nucl Med **52(Supplement 1)**(5).

Burson, J. M., G. Aguilera, et al. (1994). "Differential expression of angiotensin receptor 1A and 1B in mouse." Am J Physiol **267**(2 Pt 1): E260-7.

Campbell, D. J., D. J. Kelly, et al. (1999). "Increased bradykinin and "normal" angiotensin peptide levels in diabetic Sprague-Dawley and transgenic (mRen-2)27 rats." Kidney Int **56**(1): 211-21.

Cao, Z., F. Bonnet, et al. (2002). "Angiotensin type 2 receptor antagonism confers renal protection in a rat model of progressive renal injury." J Am Soc Nephrol **13**(7): 1773-87.

Chamberlain, R. M. and D. G. Shirley (2007). "Time course of the renal functional response to partial nephrectomy: measurements in conscious rats." Exp Physiol **92**(1): 251-62.

Chang, R. S. and V. J. Lotti (1991). "Angiotensin receptor subtypes in rat, rabbit and monkey tissues: relative distribution and species dependency." Life Sci **49**(20): 1485-90.

Cherin, E., R. Williams, et al. (2006). "Ultrahigh frame rate retrospective ultrasound microimaging and blood flow visualization in mice in vivo." Ultrasound Med Biol **32**(5): 683-91.

Chevalier, R. L. and D. L. Kaiser (1985). "Effects of acute uninephrectomy and age on renal blood flow autoregulation in the rat." Am J Physiol **249**(5 Pt 2): F672-9.

Coe, F. L. and P. R. Korty (1967). "Protein synthesis during compensatory renal hypertrophy." Am J Physiol **213**(6): 1585-9.

Cohn, J. N. and G. Tognoni (2001). "A randomized trial of the angiotensin-receptor blocker valsartan in chronic heart failure." N Engl J Med **345**(23): 1667-75.

Crowley, S. D., S. B. Gurley, et al. (2006). "Angiotensin II causes hypertension and cardiac hypertrophy through its receptors in the kidney." Proc Natl Acad Sci U S A **103**(47): 17985-90.

De Gasparo, M., K. J. Catt, et al. (2000). "International union of pharmacology, XXIII. The angiotensin II receptors." Pharmacol Rev **52**: 415-472.

Dickhout, J. G., R. E. Carlisle, et al. (2011). "Interrelationship between cardiac hypertrophy, heart failure, and chronic kidney disease: endoplasmic reticulum stress as a mediator of pathogenesis." Circ Res **108**(5): 629-42.

Dinh, D. T., A. G. Frauman, et al. (2001). "Angiotensin receptors: distribution, signalling and function." Clin Sci (Lond) **100**(5): 481-92.

Dixon, I. M., S. L. Lee, et al. (1990). "Nitrendipine binding in congestive heart failure due to myocardial infarction." Circ Res **66**: 782-788.

Dostal, D. E. and K. M. Baker (1999). "The cardiac renin-angiotensin system: conceptual, or a regulator of cardiac function?" Circ Res **85**(7): 643-50.

Edwards, N. C., C. J. Ferro, et al. (2008). "Aortic distensibility and arterial-ventricular coupling in early chronic kidney disease: a pattern resembling heart failure with preserved ejection fraction." Heart **94**(8): 1038-43.

Eguchi, S., K. Numaguchi, et al. (1998). "Calcium-dependent epidermal growth factor receptor transactivation mediates the angiotensin II-induced mitogen-activated protein kinase activation in vascular smooth muscle cells." J Biol Chem **273**(15): 8890-6.

Elkareh, J., D. J. Kennedy, et al. (2007). "Marinobufagenin stimulates fibroblast collagen production and causes fibrosis in experimental uremic cardiomyopathy." Hypertension **49**(1): 215-24.

Ferguson, S. S. (2001). "Evolving concepts in G protein-coupled receptor endocytosis: the role in receptor desensitization and signaling." Pharmacol Rev **53**(1): 1-24.

Ferrario, C. M. "Addressing the theoretical and clinical advantages of combination therapy with inhibitors of the renin-angiotensin-aldosterone system: antihypertensive effects and benefits beyond BP control." Life Sci **86**(9-10): 289-99.

Ferrario, C. M. (2009). "Addressing the theoretical and clinical advantages of combination therapy with inhibitors of the renin-angiotensin-aldosterone system: antihypertensive effects and benefits beyond BP control." Life Sci **86**(9-10): 289-99.

Foley, R. N., P. S. Parfrey, et al. (2000). "Serial change in echocardiographic parameters and cardiac failure in end-stage renal disease." J Am Soc Nephrol **11**(5): 912-6.

Fukai, T., M. R. Siegfried, et al. (1999). "Modulation of extracellular superoxide dismutase expression by angiotensin II and hypertension." Circ Res **85**(1): 23-8.

Gaborik, Z., M. Szaszak, et al. (2001). "Beta-arrestin- and dynamin-dependent endocytosis of the AT1 angiotensin receptor." Mol Pharmacol **59**(2): 239-47.

Gard, P. R. (2002). "The role of angiotensin II in cognition and behaviour." Eur J Pharmacol **438**(1-2): 1-14.

Garrido, A. M. and K. K. Griendling (2009). "NADPH oxidases and angiotensin II receptor signaling." Mol Cell Endocrinol **302**(2): 148-58.

Gobeil, F., A. Fortier, et al. (2006). "G-protein-coupled receptors signalling at the cell nucleus: an emerging paradigm." Can J Physiol Pharmacol **84**(3-4): 287-97.

Goetzl, E. J. (2007). "Diverse pathways for nuclear signaling by G protein-coupled receptors and their ligands." FASEB J **21**(3): 638-42.

Goodfriend, T. L., M. E. Elliott, et al. (1996). "Angiotensin receptors and their antagonists." N Engl J Med **334**(25): 1649-54.

Hadizad, T., J. Collins, et al. (2011 (In Press)). "[^{11}C]Methyl-losartan as a potential ligand for PET imaging angiotensin II AT_1 receptors." J Label Compd. Radiopharm.

Hadizad, T., S. A. Kirkpatrick, et al. (2009). "Novel O-[(11)C]methylated derivatives of candesartan as angiotensin II AT(1) receptor imaging ligands: radiosynthesis and ex vivo evaluation in rats." Bioorg Med Chem **17**(23): 7971-7.

Hall, A. S., G. D. Murray, et al. (1997). "Follow-up study of patients randomly allocated ramipril or placebo for heart failure after acute myocardial infarction: AIRE Extension (AIREX) Study. Acute Infarction Ramipril Efficacy." Lancet **349**(9064): 1493-7.

Harnett, J. D., P. S. Parfrey, et al. (1988). "Left ventricular hypertrophy in end-stage renal disease." Nephron **48**(2): 107-15.

Harrison-Bernard, L. M. (2009). "The renal renin-angiotensin system." Adv Physiol Educ **33**(4): 270-4.

Harrison-Bernard, L. M., L. G. Navar, et al. (1997). "Immunohistochemical localization of ANG II AT1 receptor in adult rat kidney using a monoclonal antibody." Am J Physiol **273**(1 Pt 2): F170-7.

Higuchi, T., K. Fukushima, et al. (2010). "Radionuclide imaging of angiotensin II type 1 receptor upregulation after myocardial ischemia-reperfusion injury." J Nucl Med **51**(12): 1956-61.

Higuchi, T., S. G. Nekolla, et al. (2008). "A new 18F-labeled myocardial PET tracer: myocardial uptake after permanent and transient coronary occlusion in rats." J Nucl Med **49**(10): 1715-22.

Hunyady, L., M. Bor, et al. (1994). "Identification of a cytoplasmic Ser-Thr-Leu motif that determines agonist-induced internalization of the AT1 angiotensin receptor." J Biol Chem **269**(50): 31378-82.

Ikeda, Y., T. Miura, et al. (2006). "Activation of ERK and suppression of calcineurin are interacting mechanisms of cardioprotection afforded by delta-opioid receptor activation." Basic Res Cardiol **101**(5): 418-26.

Ito, S. (2011). "Cardiorenal connection in chronic kidney disease." Clin Exp Nephrol.

Jagoda, E. M., J. J. Vaquero, et al. (2004). "Experiment assessment of mass effects in the rat: implications for small animal PET imaging." Nucl Med Biol **31**(6): 771-9.

Janke, J., M. Schupp, et al. (2006). "Angiotensin type 1 receptor antagonists induce human in-vitro adipogenesis through peroxisome proliferator-activated receptor-gamma activation." J Hypertens **24**(9): 1809-16.

Johnson, H. A. and J. M. Vera Roman (1966). "Compensatory renal enlargement. Hypertrophy versus hyperplasia." Am J Pathol **49**(1): 1-13.

Joly, E., D. Nonclercq, et al. (2005). "Differential regulation of angiotensin II receptors during renal injury and compensatory hypertrophy in the rat." Clin Exp Pharmacol Physiol **32**(4): 241-8.

Jones, B. H., M. K. Standridge, et al. (1997). "Angiotensin II increases lipogenesis in 3T3-L1 and human adipose cells." Endocrinology **138**(4): 1512-9.

Kakar, S. S., J. C. Sellers, et al. (1992). "Angiotensin II type-1 receptor subtype cDNAs: differential tissue expression and hormonal regulation." Biochem Biophys Res Commun **183**(3): 1090-6.

Kaufman, J. M., N. J. Siegel, et al. (1975). "Functional and hemodynamic adaptation to progressive renal ablation." Circ Res **36**(2): 286-93.

Kawachi, H., H. Koike, et al. (2000). "Cloning of rat nephrin: expression in developing glomeruli and in proteinuric states." Kidney Int **57**(5): 1949-61.

Kennedy, D. J., J. Elkareh, et al. (2008). "Partial nephrectomy as a model for uremic cardiomyopathy in the mouse." Am J Physiol Renal Physiol **294**(2): F450-4.

Kerr, P. G. (2006). "Renal anaemia: recent developments, innovative approaches and future directions for improved management." Nephrology (Carlton) **11**(6): 542-8.

Kestila, M., U. Lenkkeri, et al. (1998). "Positionally cloned gene for a novel glomerular protein--nephrin--is mutated in congenital nephrotic syndrome." Mol Cell **1**(4): 575-82.

Kirkpatrick, S., M. Lortie, et al. (2009). "[^{11}C]Methyl-candesartan displats binding specificity for angiotensin II AT_1 receptors." J Nucl Med **50**(Supplement 2): 301.

Klein, R., J. M. Renaud, et al. (2010). "Intra- and inter-operator repeatability of myocardial blood flow and myocardial flow reserve measurements using rubidium-82 pet and a highly automated analysis program." J Nucl Cardiol **17**(4): 600-16.

Klocke, R., W. Tian, et al. (2007). "Surgical animal models of heart failure related to coronary heart disease." Cardiovasc Res **74**(1): 29-38.

Kobori, H., A. B. Alper, Jr., et al. (2009). "Urinary angiotensinogen as a novel biomarker of the intrarenal renin-angiotensin system status in hypertensive patients." Hypertension **53**(2): 344-50.

Koike, G., E. S. Winer, et al. (1995). "Cloning, characterization, and genetic mapping of the rat type 2 angiotensin II receptor gene." Hypertension **26**(6 Pt 1): 998-1002.

Koivuviita, N., R. Tertti, et al. (2009). "Increased basal myocardial perfusion in patients with chronic kidney disease without symptomatic coronary artery disease." Nephrol Dial Transplant **24**(9): 2773-9.

Koomans, H. A., P. J. Blankestijn, et al. (2004). "Sympathetic hyperactivity in chronic renal failure: a wake-up call." J Am Soc Nephrol **15**(3): 524-37.

Koren, M. J., R. B. Devereux, et al. (1991). "Relation of left ventricular mass and geometry to morbidity and mortality in uncomplicated essential hypertension." Ann Intern Med **114**(5): 345-52.

Kubo, K., Y. Inada, et al. (1993). "Nonpeptide angiotensin II receptor antagonists. Synthesis and biological activity of benzimidazoles." J Med Chem **36**(12): 1772-84.

Leenen, F. H., B. Yuan, et al. (1999). "Brain "ouabain" and angiotensin II contribute to cardiac dysfunction after myocardial infarction." Am J Physiol **277**(5 Pt 2): H1786-92.

Lefroy, D. C., T. Crake, et al. (1996). "Angiotensin II and contraction of isolated myocytes from human, guinea pig, and infarcted rat hearts." Am J Physiol **270**(6 Pt 2): H2060-9.

Lefroy, D. C., J. Wharton, et al. (1996). "Regional changes in angiotensin II receptor density after experimental myocardial infarction." J Mol Cell Cardiol **28**(2): 429-40.

Levine, D. Z., M. Iacovitti, et al. (1997). "ANG II-dependent HCO3- reabsorption in surviving rat distal tubules: expression/activation of H(+)-ATPase." Am J Physiol **272**(6 Pt 2): F799-808.

Levy, D., K. M. Anderson, et al. (1987). "Risk of ventricular arrhythmias in left ventricular hypertrophy: the Framingham Heart Study." Am J Cardiol **60**(7): 560-5.

Li, D. Y., Y. C. Zhang, et al. (1999). "Upregulation of endothelial receptor for oxidized low-density lipoprotein (LOX-1) in cultured human coronary artery endothelial cells by angiotensin II type 1 receptor activation." Circ Res **84**(9): 1043-9.

Li, H., H. F. Li, et al. (2008). "Rab4 and Rab11 coordinately regulate the recycling of angiotensin II type I receptor as demonstrated by fluorescence resonance energy transfer microscopy." J Biomed Opt **13**(3): 031206.

Li, Z., M. Iwai, et al. (2003). "Role of AT2 receptor in the brain in regulation of blood pressure and water intake." Am J Physiol Heart Circ Physiol **284**(1): H116-21.

Liu, B. C., J. Sun, et al. (2004). "Effect of irbesartan on angiotensin II-induced hypertrophy of human proximal tubular cells." Chin Med J (Engl) **117**(4): 547-51.

Llorens-Cortes, C., B. Greenberg, et al. (1994). "Tissular expression and regulation of type 1 angiotensin II receptor subtypes by quantitative reverse transcriptase-polymerase chain reaction analysis." Hypertension **24**(5): 538-48.

Logan, J., J. S. Fowler, et al. (1990). "Graphical analysis of reversible radioligand binding from time-activity measurements applied to [N-11C-methyl]-(-)-cocaine PET studies in human subjects." J Cereb Blood Flow Metab **10**(5): 740-7.

Mackie, F. E., D. J. Campbell, et al. (2001). "Intrarenal angiotensin and bradykinin peptide levels in the remnant kidney model of renal insufficiency." Kidney Int **59**(4): 1458-65.

Maggioni, A. P., I. Anand, et al. (2002). "Effects of valsartan on morbidity and mortality in patients with heart failure not receiving angiotensin-converting enzyme inhibitors." J Am Coll Cardiol **40**(8): 1414-21.

Makino, N., T. Hata, et al. (1996). "Regression of hypertrophy after myocardial infarction is produced by the chronic blockade of angiotensin type 1 receptor in rats." J Mol Cell Cardiol **28**(3): 507-17.

Masaki, H., T. Kurihara, et al. (1998). "Cardiac-specific overexpression of angiotensin II AT2 receptor causes attenuated response to AT1 receptor-mediated pressor and chronotropic effects." J Clin Invest **101**(3): 527-35.

Mathews, W. B., H. D. Burns, et al. (1995). "Carbon-11 Labeling of a Potent, Nonpeptide, AT1-Selective Angiotensin-II Receptor Antagonist: MK-996." Journal of Labelled Compounds and Radiopharmaceuticals **XXXVI**(8): 729-737.

Mathews, W. B., S. E. Yoo, et al. (2004). "A novel radioligand for imaging the AT1 angiotensin receptor with PET." Nucl Med Biol **31**(5): 571-4.

McMurray, J. J., J. Ostergren, et al. (2003). "Effects of candesartan in patients with chronic heart failure and reduced left-ventricular systolic function taking angiotensin-converting-enzyme inhibitors: the CHARM-Added trial." Lancet **362**(9386): 767-71.

Meggs, L. G., J. Coupet, et al. (1993). "Regulation of angiotensin II receptors on ventricular myocytes after myocardial infarction in rats." Circ Res **72**(6): 1149-62.

Mehta, P. K. and K. K. Griendling (2007). "Angiotensin II cell signaling: physiological and pathological effects in the cardiovascular system." Am J Physiol Cell Physiol **292**(1): C82-97.

Miyata, N., F. Park, et al. (1999). "Distribution of angiotensin AT1 and AT2 receptor subtypes in the rat kidney." Am J Physiol **277**(3 Pt 2): F437-46.

Moriguchi, Y., K. Yogo, et al. (2011). "Left ventricular hypertrophy is associated with inflammation in sodium loaded subtotal nephrectomized rats." Biomed Res **32**(2): 83-90.

Mukherjee, A., P. Kulkarni, et al. (1982). "Evidence for the presence and characterization of angiotensin II receptors in rat anterior pituitary membranes." Endocrinology **110**(2): 665-7.

Nakajima, M., H. G. Hutchinson, et al. (1995). "The angiotensin II type 2 (AT2) receptor antagonizes the growth effects of the AT1 receptor: gain-of-function study using gene transfer." Proc Natl Acad Sci U S A **92**(23): 10663-7.

Nishikawa, K., T. Naka, et al. (1997). "Candesartan cilexetil: a review of its preclinical pharmacology." J Hum Hypertens **11 Suppl 2**: S9-17.

Noda, K., Y. H. Feng, et al. (1996). "The active state of the AT1 angiotensin receptor is generated by angiotensin II induction." Biochemistry **35**(51): 16435-42.

Noda, K., Y. Saad, et al. (1995). "Interaction of Phe8 of angiotensin II with Lys199 and His256 of AT1 receptor in agonist activation." J Biol Chem **270**(48): 28511-4.

Oestreicher, E. M., C. Guo, et al. (2006). "Estradiol increases proteinuria and angiotensin II type 1 receptor in kidneys of rats receiving L-NAME and angiotensin II." Kidney Int **70**(10): 1759-68.

Ohyama, K., Y. Yamano, et al. (1995). "Disulfide bridges in extracellular domains of angiotensin II receptor type IA." Regul Pept **57**(2): 141-7.

Opie, L. H. and M. N. Sack (2001). "Enhanced angiotensin II activity in heart failure: reevaluation of the counterregulatory hypothesis of receptor subtypes." Circ Res **88**(7): 654-8.

Pallone, T. L. (1994). "Vasoconstriction of outer medullary vasa recta by angiotensin II is modulated by prostaglandin E2." Am J Physiol **266**(6 Pt 2): F850-7.

Parmar, M. S. (2002). "Chronic renal disease." BMJ **325**(7355): 85-90.

Pendergrass, K. D., T. M. Gwathmey, et al. (2009). "The angiotensin II-AT1 receptor stimulates reactive oxygen species within the cell nucleus." Biochem Biophys Res Commun **384**(2): 149-54.

Pfeffer, M. A., E. Braunwald, et al. (1992). "Effect of captopril on mortality and morbidity in patients with left ventricular dysfunction after myocardial infarction. Results of the survival and ventricular enlargement trial. The SAVE Investigators." N Engl J Med **327**(10): 669-77.

Piecha, G., N. Koleganova, et al. (2008). "Regression of glomerulosclerosis in subtotally nephrectomized rats: effects of monotherapy with losartan, spironolactone, and their combination." Am J Physiol Renal Physiol **295**(1): F137-44.

Rosen, E. D., C. J. Walkey, et al. (2000). "Transcriptional regulation of adipogenesis." Genes Dev **14**(11): 1293-307.

Santos, L. S., E. W. Chin, et al. (2006). "Surgical reduction of the renal mass in rats: morphologic and functional analysis on the remnant kidney." Acta Cir Bras **21**(4): 252-7.

Schalekamp, M. A. and A. H. Danser (2006). "Angiotensin II production and distribution in the kidney--II. Model-based analysis of experimental data." Kidney Int **69**(9): 1553-7.

Senchenkova, E. Y., J. Russell, et al. (2010). "Angiotensin II-mediated microvascular thrombosis." Hypertension **56**(6): 1089-95.

Shah, A., H. R. Schelbert, et al. (1985). "Measurement of regional myocardial blood flow with N-13 ammonia and positron-emission tomography in intact dogs." J Am Coll Cardiol **5**(1): 92-100.

Sui, Y., H. L. Zhao, et al. (2010). "Renin-angiotensin system activation in renal adipogenesis." Am J Physiol Renal Physiol **298**(2): F391-400.

Suuronen, E. J., J. Price, et al. (2007). "Comparative effects of mesenchymal progenitor cells, endothelial progenitor cells, or their combination on myocardial infarct regeneration and cardiac function." J Thorac Cardiovasc Surg **134**(5): 1249-58.

Suzuki, K., G. D. Han, et al. (2007). "Angiotensin II type 1 and type 2 receptors play opposite roles in regulating the barrier function of kidney glomerular capillary wall." Am J Pathol **170**(6): 1841-53.

Sviglerova, J., J. Kuncova, et al. (2010). "Cardiovascular parameters in rat model of chronic renal failure induced by subtotal nephrectomy." Physiol Res **59 Suppl 1**: S81-8.

Szabo, Z., P. F. Kao, et al. (1998). "Investigation of angiotensin II/AT1 receptors with carbon-11-L-159,884: a selective AT1 antagonist." J Nucl Med **39**(7): 1209-13.

Tan, J., H. Wang, et al. (2004). "Increases in brain and cardiac AT1 receptor and ACE densities after myocardial infarct in rats." Am J Physiol Heart Circ Physiol **286**(5): H1665-71.

Tanaka, M., S. Tsuchida, et al. (1999). "Vascular response to angiotensin II is exaggerated through an upregulation of AT1 receptor in AT2 knockout mice." Biochem Biophys Res Commun **258**(1): 194-8.

Thomas, W. G., T. J. Thekkumkara, et al. (1995). "Stable expression of a truncated AT1A receptor in CHO-K1 cells. The carboxyl-terminal region directs agonist-induced internalization but not receptor signaling or desensitization." J Biol Chem **270**(1): 207-13.

Timmermans, P. B., A. T. Chiu, et al. (1992). "Angiotensin II receptor subtypes." Am J Hypertens **5**(6 Pt 1): 406-10.

Toblli, J. E., G. Cao, et al. (2008). "Heart and iron deficiency anaemia in rats with renal insufficiency: the role of hepcidin." Nephrology (Carlton) **13**(7): 636-45.

Topham, P. S., H. Kawachi, et al. (1999). "Nephritogenic mAb 5-1-6 is directed at the extracellular domain of rat nephrin." J Clin Invest **104**(11): 1559-66.

Valentin, J. P., L. A. Sechi, et al. (1997). "The renin-angiotensin system and compensatory renal hypertrophy in the rat." Am J Hypertens **10**(4 Pt 1): 397-402.

Vauquelin, G., F. Fierens, et al. (2001). "Role of basic amino acids of the human angiotensin type 1 receptor in the binding of the non-peptide antagonist candesartan." Journal of the Renin-Angiotensin-Aldosterone System **2 (Supplement 1)**: S32-S36.

Vaziri, N. D., Y. Bai, et al. (2007). "Intra-renal angiotensin II/AT1 receptor, oxidative stress, inflammation, and progressive injury in renal mass reduction." J Pharmacol Exp Ther **323**(1): 85-93.

Verjans, J., L. Hofstra, et al. (2008). "Molecular imaging of interstitial alterations after myocardial infarction." J Cardiovasc Transl Res **1**(3): 221-4.

Verjans, J. W., D. Lovhaug, et al. (2008). "Noninvasive imaging of angiotensin receptors after myocardial infarction." JACC Cardiovasc Imaging **1**(3): 354-62.

Wagenaar, L. J., A. A. Voors, et al. (2002). "Angiotensin receptors in the cardiovascular system." Can J Cardiol **18**(12): 1331-9.

Wang, Z. Q., L. J. Millatt, et al. (1999). "Differential regulation of renal angiotensin subtype AT1A and AT2 receptor protein in rats with angiotensin-dependent hypertension." Hypertension **33**(1): 96-101.

Xia, J., E. Seckin, et al. (2008). "Positron-emission tomography imaging of the angiotensin II subtype 1 receptor in swine renal artery stenosis." Hypertension **51**(2): 466-73.

Yoneda, M., H. Sanada, et al. (2005). "Differential effects of angiotensin II type-1 receptor antisense oligonucleotides on renal function in spontaneously hypertensive rats." Hypertension **46**(1): 58-65.

Young, L. S., M. C. Regan, et al. (1998). "Changes in regional renal blood flow after unilateral nephrectomy using the techniques of autoradiography and microautoradiography." J Urol **160**(3 Pt 1): 926-31.

Zhao, G., H. Zhao, et al. (2010). "Effects and mechanism of irbesartan on tubulointerstitial fibrosis in 5/6 nephrectomized rats." J Huazhong Univ Sci Technolog Med Sci **30**(1): 48-54.

Zober, T. G., W. B. Mathews, et al. (2006). "PET Imaging of the AT1 receptor with [11C]KR31173." Nucl Med Biol **33**(1): 5-13.